Journal of Radiological Protection

Official journal of the Society for Radiological Protection

PAPER • OPEN ACCESS

Re-calculation of air kerma to dose-equivalent conversion coefficients for mono-energetic photons

To cite this article: Jaroslav Šolc *et al* 2025 *J. Radiol. Prot.* **45** 021512

View the article online for updates and enhancements.

You may also like

- A systematic review on the occupational health impacts of ionising radiation exposure among healthcare professionals
Rogério Lopes, Pedro Teles and Joana Santos
- Radioactive contaminant permeation through skin: current understanding
Fernandes C S A and Sureshkumar M K
- Evaluation of dose distribution and shielding efficiency in portable intraoral x-ray device
J D Campos Méndez, S Pessoa Quesada, L Barba Ramírez et al.

This content was downloaded from IP address 95.168.107.40 on 07/04/2026 at 13:23

IOP Publishing J. Radiol. Prot. 45 (2025) 021512 https://doi.org/10.1088/1361-6498/adda56

Journal of Radiological Protection

CrossMark

OPEN ACCESS

RECEIVED
25 February 2025

REVISED
24 April 2025

ACCEPTED FOR PUBLICATION
19 May 2025

PUBLISHED
4 June 2025

Original content from this work may be used under the terms of the Creative Commons Attribution 4.0 licence.

Any further distribution of this work must maintain attribution to the author(s) and the title of the work, journal citation and DOI.

PAPER

Re-calculation of air kerma to dose-equivalent conversion coefficients for mono-energetic photons

Jaroslav Šolc[1,*], Paz Avilés Lucas[2], Luka Bakrač[3], Rolf Behrens[4], Alessia Ciccotelli[5], N Cornejo Díaz[2], Ana Fernandes[6], Steffen Ketelhut[4], Nikola Kržanović[7], Massimo Pinto[5], Teemu Siiskonen[8], Vladimír Sochor[1], Jiří Tesař[1], Joonas Tikkanen[8], Dušan B Topalović[7], Olivier Van Hoey[9], Hayo Zutz[4] and Miloš Živanović[7]

[1] Czech Metrology Institute (CMI), Okruzni 31, 638 00 Brno, Czech Republic
[2] National Metrology Laboratory for Ionising Radiation (CIEMAT), Avda. Complutense 40, 28040 Madrid, Spain
[3] Ruđer Bošković Institute (IRB), Bijenička cesta 54, 10000 Zagreb, Croatia
[4] Physikalisch-Technische Bundesanstalt (PTB), Bundesallee 100, 38116 Braunschweig, Germany
[5] Istituto Nazionale di Metrologia delle Radiazioni Ionizzanti (ENEA-INMRI), Via Anguillarese 301, 00123 Santa Maria di Galeria, (RM), Italy
[6] The Instituto Superior Técnico (IST), Av. Rovisco Pais 1, 1049-001 Lisboa, Portugal
[7] Department of Radiation and Environmental Protection, Vinča Institute of Nuclear Sciences, National Institute of the Republic of Serbia, University of Belgrade (VINS), PO Box 522, 11001 Belgrade, Serbia
[8] Radiation and Nuclear Safety Authority (STUK), Jokiniemenkuja 1, 01370 Vantaa, Finland
[9] Belgian Nuclear Research Centre (SCK CEN), Boeretang 200, B-2400 Mol, Belgium
[*] Author to whom any correspondence should be addressed.

E-mail: jaroslav.solc@cmi.gov.cz

Keywords: area dosimetry, conversion coefficients, ISO 4037 standard, Monte Carlo, MCNP, personal dosimetry, total air kerma

Supplementary material for this article is available online

Abstract

This work presents new calculations of conversion coefficients (CCs) from total air kerma to dose-equivalent quantities $H'(0.07)$, $H'(3)$, $H^*(10)$, $H_p(0.07)$, $H_p(3)$, and $H_p(10)$ for area and personal dosimetry for mono-energetic photons in the energy range from 2 keV to 50 MeV, assuming secondary charged particle equilibrium. Calculations using the Monte Carlo N-Particle® (MCNP) code were performed for a large number of photon energies with the aim of preventing errors resulting from possible improper interpolation between currently available sparsely spaced CC values, when an average CC value over a photon fluence spectrum needs to be determined. The CC values were compared with the values published in the ISO 4037-3:2019 standard. A very close agreement was achieved for the majority of CCs. Larger discrepancies were found for some CCs, often for low photon energies or large angles of radiation incidence, which were taken from older publications or when CC values were interpolated or extrapolated. Furthermore, some differences were found in the MeV energy range, which are significant for dosimeter calibrations, e.g. the presented values of CC to $H^*(10)$ for the main photon energies of ^{137}Cs and ^{60}Co radionuclides are both lower by 2.8%. Finally, it was found that the values of CCs to $H_p(0.07; E, \alpha)_{slab}$ given in ISO 4037-3:2019 were not taken correctly from the source publication. In conclusion, the CC values given in ISO 4037-3:2019 should be updated in view of the results obtained.

1. Introduction

In Publication 103 [1] of The International Commission on Radiological Protection (ICRP), the protection of human health against effects caused by ionizing radiation is based on the prevention of tissue reactions (deterministic effects) and on the limitation of the risks of cancer and hereditary effects (stochastic effects). Two risk-related dosimetric radiation protection quantities are defined. The organ-equivalent dose is used to manage and control exposure to ionizing radiation so that deterministic effects are prevented. The effective dose is used to reduce the risk of stochastic effects to the extent reasonably achievable [1]. These quantities

© 2025 The Author(s). Published on behalf of the Society for Radiological Protection by IOP Publishing Ltd

are not directly measurable. Therefore, surrogate operational quantities aimed at measurement and instrument calibration are defined in Report 39 [2] of The International Commission on Radiation Units and Measurements (ICRU) and later in ICRU Report 51 [3], providing acceptable and mostly conservative estimates of the protection quantities. Two groups of operational quantities were introduced: one for monitoring personal exposure, and one for area monitoring at workplaces and in the environment.

The methods for calibrating and determining the response of area and personal dosimeters and dose rate meters for radiological protection in x-ray and γ-ray reference radiation fields in terms of the ICRU 51 operational quantities are defined by the international standard ISO 4037 [4–7]. Primary photon dosimetry is described in terms of air kerma. Conversion to the operational quantity of interest is realized by multiplying the air kerma with a conversion coefficient (CC) specific to the given radiation quality. This allows the instrument response to be determined in terms of the operational quantity of interest. ISO 4037-3:2019 (subsequently referred to as ISO 4037-3) provides tables with CC values. Newly published CCs in the literature (e.g. [8]) were used to extend the range of CCs presented in the previous version [9]. CC values can be directly taken from ISO 4037-3 when matched reference radiation fields are established according to the specific requirements of ISO 4037-1 [4]. Otherwise, the CC value has to be obtained either by the direct measurement of the operational quantity under consideration using a secondary standard compliant with the requirements defined in [5], or by x-ray spectrometry. In the latter case, the CC values for mono-energetic photons taken from [6] should be used to calculate the average CC value for the given radiation quality from the measured spectral distribution of photon fluence [10–12].

CC values for mono-energetic photons in [6] were taken from various sources available before its publication, mainly adopted from ICRU 57 [13] but also from others. This inevitably resulted in a data set of differently determined values; some of them were obtained with air kerma factors and a phantom located in a vacuum, while others considered electron transport in air [14]. Some were obtained using collision kerma only [15], whereas others were derived using total air kerma, or such information was not mentioned at all. Finally, some references in ICRU 57 are unpublished. Furthermore, for several operational quantities, some tabulated mono-energetic CC values were interpolated from the original data and extrapolated at very low photon energies. In addition, this might increase the uncertainty. To obtain a mean CC value for the x-ray fluence spectrum of interest, tabulated mono-energetic CC values from ISO 4037-3 have to be interpolated, which may lead to an inaccurate value if an unsuitable interpolation method is used, as was previously investigated in [16]. In line with the recommendation given in ICRU 57 [13], ICRP 116 [17] suggests a four-point (cubic) Lagrangian interpolation formula in a linear–log graph scale. However, for some CC values, namely for low-energy photons, a linear–linear interpolation was considered more appropriate [16] but this is also questionable. As suggested in [18] and later applied by the same author [8, 19], an interpolation method should be chosen appropriately and checked to avoid oscillations between the sparsely spaced tabulated data points. This is especially important for narrow x-ray radiation qualities [4], where the whole spectrum may fit in between just two or three consecutive tabulated CC data points.

The aim of this work is to provide a new, consistent determination of mono-energetic values of CCs for all operational quantities considered in ISO 4037-3 and for a much larger number of photon energies. This removes the need to test interpolation methods to avoid errors resulting from possible improper interpolation between tabulated mono-energetic CC values.

The photon energies from 2 keV to 50 MeV considered in this work encompass the whole energy range for testing and calibration of instruments in x-ray radiation, ^{137}Cs, ^{60}Co, and high-energy fields. The impact of the newly calculated mono-energetic CC values on the CC values for the reference radiation qualities defined in [4] will be the scope of another publication.

A minor goal of this work is to answer the question of which data in ISO 4037-3 for mono-energetic photons provide CCs from the total air kerma and which are from the collision air kerma. This has been discussed in the past, e.g. section 3.4 in [19], 'Collisional air kerma or total air kerma' in [18] and 'Total air kerma or collisional air kerma' in [8]. The presented work provides the answers.

New operational quantities, for which ICRP/ICRU reference phantoms of the human body [20] are used as a basis for calculations, were proposed in ICRU Report 95 [21]. It was published in 2020 and aimed to replace the current operational quantities considered in ISO 4037. The recommended new operational quantities are the personal dose and ambient dose, as measures of the effective dose used in the limitation and optimization of protection against stochastic effects, and the personal absorbed dose and directional absorbed dose, as measures of the local absorbed dose to the lens of the eye and to local skin to set limits to prevent deterministic effects [21]. However, the implementation of ICRU 95 quantities in practice is complicated, especially for manufacturers of measuring devices, because it would usually require mechanical and software modifications of the dosimetry systems [22]. For some combinations of dosimetry systems, new quantities, particle types, and energy range modifications are even impossible without an increase in the measurement uncertainty and a significant rise in the cost of the detector [23–25]. The authors of ICRU 95

anticipate that the time required for the incorporation of recommendations into safety standards and legislation could be as long as 20 years. Therefore, the current personal and area operational quantities for radiation protection are still relevant, and their improvement is of interest.

The effort leading to the presented results was driven by discrepancies in ISO 4037-3 data found during the work on a joint European metrological research project entitled 'Harmonisation, update and implementation of standards related to radiation protection dosemeters for photon radiation' [26] (22NRM07 GuideRadPROS). The three-year project, started in 2023, is led by the Finnish radiation and nuclear safety authority (STUK) and aims to provide guidance and protocols to metrology institutes, standardization bodies, and regulators for a consistent and harmonized approach to radiation protection measurements and calibrations following the ISO 4037 standard series [4–7].

2. Materials and methods

2.1. Basic terms

The absorbed dose in a given volume of matter, D, in units of Gy, is the quotient of the mean energy imparted by ionizing radiation to this volume of matter and its mass [27].

Charged-particle equilibrium (CPE) at a point (volume of interest) exists if the distribution of the charged-particle radiance with respect to energy is constant within distances equal to the maximum charged-particle range [22], i.e. throughout a sufficiently small volume. Therefore, the sums of the energies (excluding rest energies) of the charged particles entering and leaving the volume are equal [17].

Kerma, K, is the quotient of the mean sum of the initial kinetic energies of all the charged particles liberated in a given volume of matter by the incident uncharged particles, and the mass of matter within this volume [27]. It can also be calculated from equation (1), where Φ is the uncharged particle fluence, E is the uncharged particle energy, $\frac{\mu_{en}}{\rho}$ is the mass energy absorption coefficient of the material for uncharged particles of energy E, and g is the fraction of the energy of the liberated secondary charged particles that is lost by radiative processes.

$$K = \Phi \cdot E \cdot \frac{\mu_{en}}{\rho} \frac{1}{(1-g)} \tag{1}$$

K, also referred to as the total kerma, can be divided into the collision kerma, K_{coll}, and the radiative kerma, K_{rad}, according to equation (2). K_{coll} is realized by ionization and excitation energy losses of charged particles, while K_{rad} accounts for radiative energy losses of charged particles. K_{coll} is measurable with ionization chambers and approaches the absorbed dose to the degree that CPE exists, that radiative losses are negligible, and that the kinetic energy of the uncharged particles is large compared to the binding energy of the liberated charged particles [27],

$$K = K_{coll} + K_{rad};\ K_{coll} = K \cdot (1-g) \approx D;\ K_{rad} = K \cdot g. \tag{2}$$

Often, Monte Carlo (MC) radiation transport codes take advantage of $K_{coll} \approx D$, and the absorbed dose is determined using the kerma approximation, which usually allows for much faster calculations because time-consuming electron transport is not required. In ISO 4037-3, the CCs are defined for free-in-air air kerma, K_a, with the assumption of negligible radiative kerma up to the energy of ^{60}Co radiation (with an assumed mean energy of 1.25 MeV).

The dose equivalent, H, in units of Sv, is given by the product of D at a point in tissue or organ and the quality factor Q, which is equal to 1 Sv Gy^{-1} for photons [3]. The selection of a phantom, the depth in the phantom, and the radiation field define the exposure situation and distinguish between different dose-equivalent operational quantities.

ICRU 4-element tissue has a density of 1.0 g·cm^{-3} and a mass composition of 76.2% oxygen, 11.1% carbon, 10.1% hydrogen, and 2.6% nitrogen [2].

The ICRU sphere is defined as a sphere with a diameter of 30 cm filled with ICRU 4-element tissue. It is anticipated that this phantom adequately approximates the scattering and attenuation of radiation fields in the human body [2].

An expanded radiation field is defined as a hypothetical field in which the fluence and its direction and energy distribution have the same values throughout the whole volume of interest as in the actual field at the point of [2]. An expanded and aligned radiation field is obtained if all radiation is aligned in the expanded radiation field so that it is opposed to a radius vector Ω specified for the ICRU sphere [2]. See also the visualizations in [28].

2.2. Operational quantities

Each quantity represents the dose equivalent at a point at a given depth of a specified phantom irradiated with an expanded or with an expanded and aligned radiation field.

2.2.1. Area dosimetry

The relevant quantities for area dosimetry used for workplace and environmental monitoring are the directional dose equivalent, $H'(d, \Omega)$, and the ambient dose equivalent, $H^*(10)$. $H'(d, \Omega)$ at a point in a radiation field is the dose equivalent that would be produced by the corresponding expanded field in the ICRU sphere at a depth d on a radius in a specified direction Ω. For unidirectional incidence of the radiation beams (during calibration and calculation of CC values) Ω is replaced by α, the angle between the direction Ω and the radius opposing the direction of the field. $H'(3)$ and $H'(0.07)$ are the estimates for organ-equivalent doses to the lens of the eye at a depth of 3 mm and local skin at a depth of 0.07 mm, which set limits to prevent deterministic effects. $H^*(10)$ at a point in a radiation field is the dose equivalent that would be produced by the corresponding expanded and aligned field in the ICRU sphere at a depth of 10 mm on the radius opposing the direction of the aligned field. $H^*(10)$ is an estimate of the effective dose, on which limits are set to minimize stochastic effects [17].

2.2.2. Personal dosimetry

The relevant quantity for personal dosimetry used for individual monitoring is the personal dose equivalent, $H_p(d)$. It is the dose equivalent in soft tissue at a depth of d mm below a specified point on the human body, $H_p(d)$. The specified point is usually given by the position where the individual dosimeter is worn [17]. $H_p(3)$ and $H_p(0.07)$ are the estimates for organ-equivalent doses to the lens of the eye and local skin at the respective depths of 3 mm and 0.07 mm. $H_p(10)$ is an estimate of the effective dose. For the purpose of instrument calibration and testing, the body is approximated by a phantom suitable for the intended purpose of the instrument. The following phantoms are defined for personal dosimetry: an ICRU slab phantom [29] (width × height × depth = 30 cm × 30 cm × 15 cm) for $H_p(0.07; \alpha)$ and $H_p(10; \alpha)$ in the whole body, a cylindrical phantom [30] (height × diameter = 20 cm × Ø 20 cm) for $H_p(3; \alpha)$ in the eye lens, a rod phantom [31] (height × diameter = 30 cm × Ø 1.9 cm) for $H_p(0.07)$ in the fingers, and a pillar phantom [32] (height × diameter = 30 cm × Ø 7.3 cm) for $H_p(0.07)$ in the wrists and ankles. All phantoms consist of the ICRU 4-element tissue. However, the ICRU 4-element tissue cannot be fabricated [33]; therefore, to mimic their backscatter for dosimeter calibrations, the phantoms are substituted by polymethylmethacrylate (PMMA) phantoms [6] of the same outer dimensions but filled with water, except for the rod, which is solid PMMA. Nevertheless, no correction factors are applied for possible differences in back-scatter properties as they are considered to be negligible [6]. The ICRU 4-element tissue is used in all MC simulations performed in this work.

2.3. Conversion coefficients

In ISO 4037-3 [6], the operational quantities, $H(d)$, are determined as a product of the total air kerma, K_a, and the appropriate CC, h_K, specific to the operational quantity and the radiation quality under consideration. The CC values are provided therein for mono-energetic photons and for reference radiation fields.

2.4. Secondary charged particle equilibrium

In line with the assumptions of ISO 4037-3, all CCs presented in this paper were calculated using the kerma approximation method and are valid under secondary CPE and hence completed build-up. For tests of instruments according to [5] or [34] and using the CC values in [6] or in this paper, CPE is achieved by adding a layer of PMMA of sufficient thickness directly in front of the instrument or dosimeter-phantom setup [34]. Otherwise, the deviations of the dose from its value under CPE depend on the experimental setup being used, which precludes the use of universally applicable CC values [6]. A layer of 3 mm has been found to be sufficient to establish CPE for the radiation fields of ^{137}Cs and ^{60}Co [35], while a layer of 25 mm is necessary for the high-energy radiation fields R–C and R–F with 4.4 MeV and 6–7 MeV [36]. The modification of the radiation field induced by the 3 mm PMMA plate is considered negligible for ^{137}Cs and ^{60}Co. On the other hand, the absorption in the 25 mm PMMA plate is not negligible for the R–C and R–F fields and it is treated with a correction $k_{PMMA} < 1$ in ISO 4037-3 [6]. In the case of filtered x-ray radiation qualities, the use of the PMMA plate is not necessary [6]. The presented work did not consider any build-up plate as CPE was assumed for all photon energies whilst undertaking the calculations by turning off the electron transport; see below.

2.5. Renormalized or unrenormalized Scofield photoeffect cross-sections

The unrenormalized Scofield photoeffect data have been adopted for a long time, for example, in the XCOM database [37] and the electron photon interaction cross-sections (EPICS) [38] used by the Monte Carlo N-Particle® (MCNP) software. On the other hand, the unrenormalized data modified with a normalization screening correction [39], referred to as renormalized photoeffect cross-sections, have been more recently adopted in PENELOPE MC software [40] for all elements, and were introduced to a more general audience in the ICRU 90 publication [41] for air, water, and carbon (graphite) only, but not for the ICRU 4-element tissue. The consideration of renormalized photoeffect cross-sections decreases the total cross-section in air by about 2.5%, 1.5%, 0.5%, and 0.1% for photon energies of 20 keV, 54 keV, 85 keV, and 160 keV, respectively, which may, ultimately, influence the CC values. For a detailed discussion of the renormalization of photoeffect cross-sections, the reader is referred to chapter 6.1 in the ICRU 90 report [41].

ICRU 90 presents a comparison of measurements and theoretical predictions of the total mass attenuation coefficient in air, $\left(\frac{\mu}{\rho}\right)_{\text{air}}$, indicating that, in most cases, a better agreement can be obtained with renormalized photoeffect cross-sections. However, the results were not fully convincing, leading the ICRU 90 authors to not finally recommend the use of renormalized cross-sections. Eventually, the authors of ICRU 95 did so by providing fluence to air kerma CCs for renormalized cross-sections (table A.6 in [21]). Similarly, the consultative committee for ionizing radiation (CCRI(I)) accepted a recommendation of an ad hoc committee formed from CCRI(I) representatives with the goal of reviewing ICRU Report 90 and making recommendations for its implementation. The committee concluded that a general recommendation to adopt renormalized cross-sections seemed appropriate, but allowed space for metrology institutes to evaluate the impact of their choice of cross-sections, if appropriate [42].

A further discussion on the application of a normalization screening correction was presented in a document dedicated to EPICS cross-section data [43]. Therein, it was noted that the experimental data are scarce and often contradictory; therefore, it is not clear whether or not the renormalization should be applied, and it may take a long time to reach a final decision on that question. Thus, the author of [43] concluded that the 2017 update of the EPICS database should keep unrenormalized data. This decision is still valid [44].

Due to the unclear situation, we aim to solve this ambiguity with a new investigation at the international level to finally decide which photoeffect cross-sections to use, both globally and for specific elements [45]. As mentioned above, further investigations were also recommended in [42].

For these reasons, in this work, the unrenormalized XCOM cross-section library was used for both air and ICRU 4-element tissue.

2.6. Potential photon-neutron contribution

As the CCs were calculated for photon energies up to 50 MeV, photo-neutrons being produced in the ICRU 4-element tissue phantoms could potentially contribute to the absorbed dose. This could, however, be ruled out, as calculations made earlier in human-like (tissue) phantoms showed no significant contributions; see section 'Simulations' in [46].

2.7. MC radiation transport simulations

2.7.1. General setting

MC radiation transport simulations were carried out by means of the general-purpose code MCNPX 2.7.E [47] for the coupled transport of ionizing radiation particles. However, only photons were transported in the simulations using the electron-photon relaxation library EPRDATA14 [48] supplied by the MCNP developers. The library is based on EPICS2014 data, where the cross-section tables for the interaction of photons with matter were taken from the evaluated photon data library, '97 Version (EPDL97) [49]. A rough estimate of the maximum uncertainty of EPDL97 data is 5%, 2%, and 1–2% for photons with an energy of 1–5 keV, 5–100 keV, and 0.1–10 MeV, respectively [49]. The photon energy cutoff was 1 keV. A planar circular or rectangular source, as appropriate for the given phantom, created an expanded and aligned radiation field of mono-energetic photons by emitting a unidirectional beam toward the phantom. The beam was wide enough to cover the whole cross-section of the phantom, even if the phantom was rotated (see figures 1 and 2). The phantom was surrounded by a vacuum. No material was included in between the source and the phantom, except for an air layer 0.1 μm thick for the purpose of K_a calculation validation (section 2.7.7).

Every simulation run generated 3×10^{10} primary particles, except for those with a slab phantom when the run was terminated after dropping the statistical uncertainty, u, below 0.1%. Many CCs were calculated in one run, which did not allow the same statistical uncertainty for all CC values to be reached. Therefore, u of the calculated results varied depending on the photon energy, angle of radiation incidence, phantom geometry, and the size of the scoring volume, but typically did not exceed 0.1% for the slab phantom and 0.05% for other phantoms. Larger u resulted in the ICRU sphere at $\alpha = 180°$ ($u \lesssim 0.5\%$, but mostly

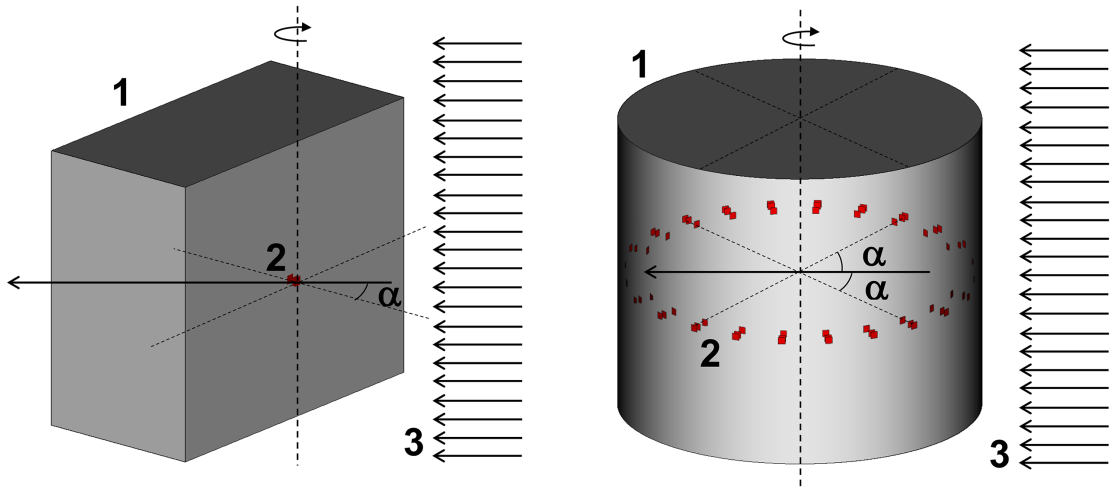

Figure 1. Schematic visualizations of the Monte Carlo models of the ICRU slab (left) and the cylinder (right) phantoms. 1—the phantom, 2—scoring volumes (red), 3—expanded and aligned radiation field.

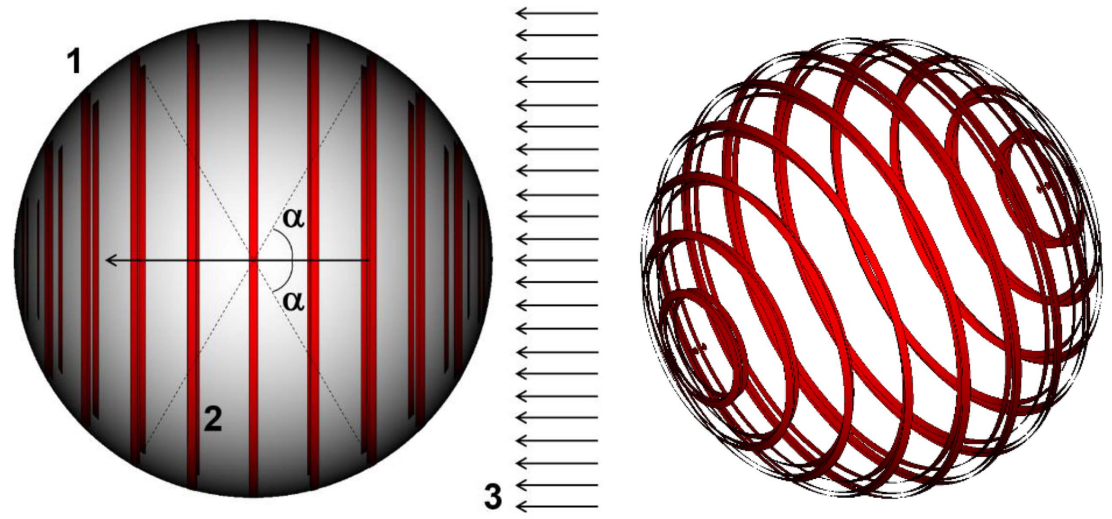

Figure 2. Schematic visualization of the MC model of the ICRU sphere (left). 1—the ICRU sphere, 2—scoring volumes (red), 3—expanded and aligned radiation field. Scoring volumes only are presented also in the right-hand side figure.

$u < 0.1\%$), in the cylinder phantom at $\alpha = 90°$ ($u \lesssim 1\%$, but mostly $u < 0.3\%$), and when the CC value was lower than about 0.01 Sv Gy^{-1}.

2.7.2. Phantom models

All numerical phantoms were composed of ICRU 4-element tissue with a density of 1.0 g·cm^{-3}. Their dimensions matched the physical phantom definitions presented in section 2.2.2. Visualizations of the ICRU slab and the cylinder phantoms are presented in figure 1. A visualization of the ICRU sphere model is shown in figure 2. The slab phantom rotational axis was vertical, passing through the geometrical center of the front surface. The shapes and sizes of the scoring volumes are given in the following sections.

2.7.3. Air kerma scoring

The total air kerma, K_a, per source photon was determined analytically according to equation (1) from the photon fluence, obtained as the reciprocal value of the source area, radiative energy losses in air, g_a, used in [21] taken from [50], and the XCOM unrenormalized values of $\frac{\mu_{en}}{\rho}$ for air and mono-energetic photons from ICRU 90 [41] (table 6.6a therein). The $\frac{\mu_{en}}{\rho}$ and g_a values for photon energies not stated in the tables were interpolated using a four-point Lagrange polynomial in log–log scale.

2.7.4. Absorbed dose scoring

The absorbed dose, D, per source photon in the ICRU 4-element tissue phantoms was realized using the F6-type photon tally, which is the photon track-length estimator of energy deposition averaged over a volume. Unrenormalized values of $\frac{\mu}{\rho}$ and $\frac{\mu_{en}}{\rho}$ [51] were used; see appendix B for details. Radiative energy losses were estimated in the MC runs from the cross-section for the production of bremsstrahlung photons taken from the el03 electron library [52] even when the electron transport was turned off [53].

Independently of the phantom shape, the thickness of scoring volumes was 1 μm at 70 μm depth and 10 μm at 3 mm and 10 mm depths. The thicknesses were chosen to be much smaller than the depth and smaller than those used in [54].

In the slab phantom, there were three rectangular scoring volumes centered on the slab central axis (parallel to the aligned photon field) at depths of 70 μm, 3 mm, and 10 mm. The length of the rectangular side was 1 cm. One simulation for each combination of the photon energy and the angle of phantom rotation was required to obtain the dose at all three depths.

In the cylindrical phantoms (cylinder, pillar, and rod) and the ICRU sphere, there were 13 scoring volumes for each depth representing angles of phantom rotation (or, equivalently, the direction of radiation incidence) from 0° to 180° in steps of 15°. Only one simulation run per photon energy was needed to calculate D at all depths and for all rotation angles due to the axial symmetry of the phantoms. Rotation around the main axis of the cylindrical phantoms was assumed. The number of combinations of angles and depths exceeds those presented in ISO 4037-3. However, D at extra angles and depths was calculated at no additional cost to the computational time. In the cylindrical phantoms, the scoring volumes were parts of an annulus around the main cylindrical axis with a height of 4 mm and limited by the angles $\Delta\alpha \pm 1.14°$ around the nominal rotation angle α (figure 1). Due to the phantom axial symmetry, D in volumes positioned at opposite angles $+\alpha$ and $-\alpha$ was scored together to double the statistics. In the ICRU sphere, the scoring volumes at all angles except 0° and 180° were annuli around the radius opposing the direction of the aligned field limited by angles $\Delta\alpha \pm 1.0°$ around the nominal angle α (figure 2). At the angles 0° and 180°, the scoring volumes were truncated cones with a vertex angle of 3°. Based on the discussion about the scoring volume size in [54], the extension $\Delta\alpha$ around the nominal value of the angle α was chosen to be much smaller than the α step and also smaller than that used in [54] to assure that the $\Delta\alpha$ does not influence the CC values.

2.7.5. Energy steps

CC values were calculated for the following photon energies: 1 keV steps between 2 keV to 20 keV, with 2 keV steps up to 60 keV, with 5 keV steps up to 100 keV, with 10 keV steps up to 200 keV, and 51 additional photon energies up to 50 MeV selected so as to include (but not be restricted to) the energies stated in ICRU 95 [21] (table A.6 therein). For the chosen energy steps, it was verified that the type of interpolation had an insignificant influence (usually $\lesssim 0.1\%$) on the CC value.

2.7.6. Calculation of CCs

From the quantities $K_a\,(E)$ in air for mono-energetic photons of energy E, and $D\,(d;\,E,\,\alpha)$ in ICRU tissue at the depth d in the given phantom rotated by the angle α, the CC $h_K\,(d;E,\alpha)$ was calculated according to equation (3), where $Q = 1$ Sv Gy^{-1}.

$$h_K\,(d;E,\alpha) = \frac{Q \cdot D\,(d;E,\alpha)}{K_a\,(E)}. \tag{3}$$

2.7.7. Internal checks and external validation

Two 'internal' checks and one 'external' validation were performed to verify the MC simulations.

The first internal check was focused on the calculation of K_a. The total air kerma per fluence, K_a/Φ, of primary mono-energetic photons determined by equation (1) was verified by comparison with K_a/Φ calculated internally by MCNP. Φ and K_a were both obtained using F4-type tallies in a 0.1 μm thin air layer located just in front of the photon source. The F4-type tally scores an average Φ in a volume calculated from the photon track length in the volume. K_a was derived during the simulation by applying tally multipliers to convert Φ of primary photons to the total K_a using the EPRDATA14 cross-section library. See appendix B for an explanation of this definition.

The second internal check focused on the method of calculation of D in the phantom. Testing of several tallies, simulation setups, and two versions of the MCNP code against the detailed dose calculation with electron transport turned on, and the justification of the tally selection, are presented in appendix B.

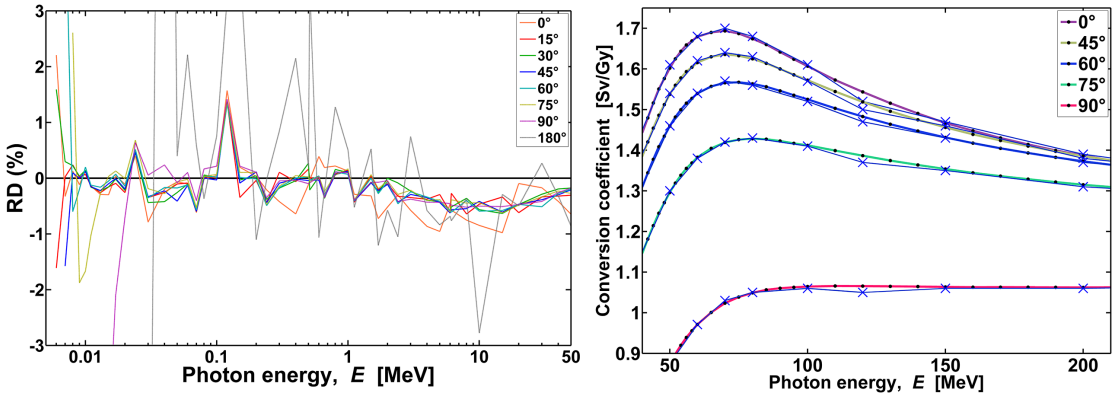

Figure 3. Left: RD between $h'_K(3; E, \alpha)$ calculated in this work (h_{MCNP}) and in [54] (h_{EGS}) for various rotation angles α for mono-energetic photons; RD = h_{MCNP}/h_{EGS}—1. Right: Systematic deviation between h_{MCNP} (dots) and h_{EGS} (crosses) for 120 keV photons, presented for selected α only.

Finally, the external validation was performed by comparing the $h'_K(3; E, \alpha)$ values calculated in this work with those calculated in [54] for collision air kerma using the EGSnrc MC code [55]. For the purpose of the comparison, radiative energy losses in air, g_a, used in the presented work were applied to the data from [54], i.e. they were multiplied with $(1-g_a)$. That work used the same idea for scoring volumes; however, in both works the MC codes, cross-section data, and the thickness and the width of the scoring volumes differed.

3. Results and discussion

3.1. Internal checks and external validation of MC calculations

K_a/Φ values calculated with MCNP and those obtained using equation (1) were compared. Their relative difference (RD), expressed as the RD of CC values, is shown in section 3.5. An RD within ±0.3% in the whole energy range demonstrates that the radiation field geometry was correctly set up and the MCNP cross-sections were correctly used. It is assumed that the obtained RD are dominated by the difference in g_a values, interpolation between tabulated cross-section data, and MCNP code treatment of available cross-section data when calculating the selected tally.

The results of dose testing in tissue calculations are summarized in appendix B. The selected tally for dose calculations was the F6:P tally derived using photon-only transport. It is presented that the systematic uncertainty given by the difference between the dose obtained with the *F8-type tally and the F6:P-type tally with electron transport turned off does not exceed 1.2%.

Comparison of the RD of $h'_K(3; E, \alpha)$ values calculated in this work and those presented in [54] (table A2 therein), corrected by the $(1–g_a)$ values used in this work, is shown in figure 3. The RD typically varied between −1% and +0.5%. This RD can be attributed to statistical uncertainties of MC simulations ('much smaller than 1%' in [54] and $u < 0.15\%$ (or $u < 0.5\%$ for $\alpha = 180°$) in this work if $h'_K(3; E, \alpha) > 0.01$ Sv/Gy), cross-section tables, interpolation of cross-section values, and differences in MC codes. An RD of 1–2% was observed at the energy of 120 keV at all angles. The reason was the difference of about 1.4% between the interpolation result for this specific energy if calculated using a four-point log–log interpolation, as in this work, or with the two-point log–log interpolation used in [54] (table A1 therein) and also in ICRU 95 [21] (table A.6 therein). The two-point log–log interpolation result was applied to derive K_a/Φ and, accordingly, the corresponding CC values in [54]. The slight deviation of the values from the smooth line in the plots in figure 3 (right) indicates that the four-point log–log interpolation provides more consistent results for an energy of 120 keV.

The very good agreement with the literature data [54] validates the MC model and the methodology used in this paper.

Finally, as published in [54], the influence of the size of scoring volumes was discussed, and it was concluded that no systematic deviations from the calculations with the original scoring volumes (a thickness of 20 μm and a maximum width of about 10 mm) were observed at the reference depth of 3 mm. Because the scoring volumes used in the presented work were smaller, the conclusions made in [54] are valid for this work as well.

3.2. Conversion coefficients for area dosimetry

3.2.1. $h'_K(0.07; E, \alpha)$

The calculated values of $h'_K(0.07; E, \alpha)$ from K_a to $H'(0.07)$ for mono-energetic and parallel photon radiation and angles of incidence α stated in ISO 4037–3 [6] are presented in figure C1 and table D1 in appendixes C and D, respectively. The mentioned figure also shows the data used in ISO 4037–3, which were taken in the limited range up to 1.25 MeV from ICRU 57 [13], which adopted the original results from [56]. The source of the interpolated CC values used in [6] is not clear. Referenced works are [16] and [57]. However, [57] does not include $h'_K(0.07; E, \alpha)$ for mono-energetic photons. In addition, ISO 4037-3 states some of the interpolated CC values given in [16], while another interpolated CC values, and all extrapolated CC values presented there are different.

The RD between the CC values in ISO 4037-3 and in the presented work varies within ±3% for $E \geqslant 10$ keV and $\alpha \leqslant 60°$. For $E < 10$ keV or $\alpha > 60°$, the RD is much larger. Obviously, below 10 keV the discrepancy was caused by the two-point linear–linear interpolation applied on the ICRU 57 data in [16]. At $\alpha \geqslant 75°$ the discrepancy might be caused by larger statistical uncertainties of the ICRU 57 data, as suggested in [54], and by averaging of the calculated absorbed dose over the dose gradients in larger scoring volumes being used in calculations in [56] and adopted by ICRU 57. The latter is especially the case for $\alpha = 90°$, as already noted by other authors [54, 58].

The $h'_K(0.07; E, \alpha)$ values cited in ICRU 57 were derived for collision air kerma [56]. This was confirmed by comparison of the CC values for $E = 10$ MeV and $\alpha = 0°$, which are 1.10 Sv/Gy in ICRU 57 (table A.23 therein) and 1.065 Sv Gy^{-1} in this work. Their RD of 3.2% is much larger than the RD for other energies. This is explained by a g_a value equal to 0.0373 ($(1–g_a)^{-1} = 1.039$) used in the presented work for the photon energy of 10 MeV, whereas ICRU 57 data were adopted by ISO 4037–3 without a correction for radiative energy losses, as only results up to 1.25 MeV were used for $h'_K(0.07; E, \alpha)$.

3.2.2. $h'_K(3; E, \alpha)$

The calculated values of $h'_K(3; E, \alpha)$ from K_a to $H'(3)$ for mono-energetic and parallel photon radiation and angles of incidence α stated in ISO 4037-3 [6] are presented in figure C2 and table D2 in appendixes C and D, respectively. The mentioned figure also shows the ISO 4037-3 data, which uses the results from [54] derived using collision air kerma. In the limited range up to 10 MeV adopted in [6], the original results were recalculated into total air kerma by applying g_a values from [5] determined according to [59]. Within this energy range, the tabulated g_a values [5] matched the g_a values used in the presented paper. The original data were used for the validation of the MC model in the presented work, and the RDs were already analyzed in section 3.1. Therefore, any difference deviating from the results presented in figure 3 could be caused by the rounding to only three significant digits in [6].

3.2.3. $h^*_K(10; E)$

The calculated values of $h^*_K(10; E)$ from K_a to $H^*(10)$ for mono-energetic and parallel photon radiation are presented in figure C3 and table D3 in appendixes C and D, respectively. The mentioned figure also shows the data used in ISO 4037-3 [6] taken from [13] and [16]. The RD of the CC values from ISO 4037-3 to those of the presented work varied within ±3% for $E \geqslant 15$ keV. Below 15 keV, where $h^*_K(10; E) < 0.2$ Sv Gy^{-1}, the differences were larger.

The ISO 4037-3 data were taken from ICRU 57 [13], which were obtained from ICRU 47 [29] applying the updated $\frac{\mu_{en}}{\rho}$ data. The CC values in ICRU 47 were compiled from several MC simulations and experiments published between 1979 and 1985. These data sets were evaluated in [60] and [14]. To obtain the mean $h^*_K(10; E)$ values, the first work calculated an average weighted by statistical and systematic uncertainties subsequently fitted with spline functions. The latter work proposed an empirical analytic function of energy valid above 20 keV. For $E \leqslant 20$ keV, an average of the three results available in the literature at that time was used. Mean $h^*_K(10; E)$ resulted from both evaluations differ by ±2% up to 3 MeV, which is less than the uncertainties in the calculations [29]. Therefore, the analytic function was adopted for the calculation of the $h^*_K(10; E)$ values tabulated in ICRU 47 and later adopted by ICRU 57. For a full discussion and references to the original papers, see [13] and [29]. The analytic function was derived in [14] and was also presented in [29] and [28].

Although ICRU 47 gives the equation for the total air kerma (section A.2.1 in [29]), the provided $h^*_K(10; E)$ values derived from the analytic function, and subsequently adopted by ICRU 57, were determined for collision air kerma. This can be traced to original works, e.g. [61], and it is also obvious by comparing the $h^*_K(10; E)$ value for $E = 10$ MeV of 1.10 Sv/Gy and 1.05 Sv/Gy given in ICRU 57 and in the

presented work, respectively. The resulting RD of 4.5% is largely outside the range of RD at energies $\lesssim$1.5 MeV, and it corresponds rather to the radiative energy loss of $g_a = 0.0373$ ($(1–g_a)^{-1} = 1.039$) for 10 MeV photons. Also, ISO 4037-3 states that g_a values from [5] were applied to the $h^*_K(10; E)$ values when they were adopted from ICRU 57.

In conclusion, the RDs between the presented and ISO 4037-3 $h^*_K(10; E)$ values are in line with the RD of ∼2% between previous evaluations, which ICRU 57 considered as a good agreement [13]. The specific consequence is the deviation of the presented and ISO 4037–3 $h^*_K(10; E)$ values for ^{137}Cs and ^{60}Co radionuclides commonly used for dosimeter calibrations. The RD observed is −2.8%. The presented $h^*_K(10; E)$ is 1.176 Sv Gy^{-1} for mono-energetic 662 keV photons of ^{137}Cs and 1.128 Sv/Gy for 1.25 MeV photons of ^{60}Co (approximate average of dominant 1.17 MeV and 1.33 MeV photons emitted by ^{60}Co), while the ISO 4037-3 gives 1.21 Sv Gy^{-1} and 1.16 Sv Gy^{-1} for ^{137}Cs and ^{60}Co, respectively [6]. It is anticipated that these differences will also propagate average $h^*_K(10; E)$ values calculated for a realistic energy fluence spectrum of ^{137}Cs and ^{60}Co.

3.3. Conversion coefficients for personal dosimetry

3.3.1. $h_{pK}(0.07; E)_{rod}$

The calculated values of $h_{pK}(0.07; E)_{rod}$ from K_a to $H_p(0.07)$ for mono-energetic and parallel photon radiation and the rod phantom are presented in figure C4 and table D4 in appendixes C and D, respectively. The mentioned figure also shows the data used in ISO 4037-3 taken from [15] and [16]. Except for 3 keV, the RD for the presented work varied within −0.5% and +1.5%, which can be attributed to the statistical uncertainties of MC simulations ($u = 0.1$–1.0% in [15], table 1 therein), the rounding to only three significant digits in [6], the interpolation used by [16], and the neglection of radiative energy losses. An RD reaching 3.5% was found for the lowest photon energy of 3 keV. The CC value for this energy used in [6] was an extrapolated value from [16]. $h_{pK}(0.07; E)_{rod}$ values were given for collision air kerma in [15] and were adopted by [6] without any change, as the maximum E is 1.25 MeV.

3.3.2. $h_{pK}(0.07; E)_{pill}$

The calculated values of $h_{pK}(0.07; E)_{pill}$ from K_a to $H_p(0.07)$ for mono-energetic and parallel photon radiation and the pillar phantom are presented in figure C5 and table D5 in appendixes C and D, respectively. The mentioned figure also shows the data used in ISO 4037-3 taken from [15]. A very good agreement was observed, with the RD to the presented work varying between −0.6% and +1.1%. These limited differences can be attributed to the statistical uncertainties of MC simulations ($u = 0.1$–0.7% in [15], table 1 therein), the rounding to only three significant digits in [6], and neglection of radiative energy losses. $h_{pK}(0.07; E)_{pill}$ values were given for collision air kerma in [15] and were adopted by [6] without any change, as the maximum E is 1.25 MeV.

3.3.3. $h_{pK}(0.07; E, \alpha)_{slab}$

The calculated values of $h_{pK}(0.07; E, \alpha)_{slab}$ from K_a to $H_p(0.07)$ for mono-energetic and parallel photon radiation, the slab phantom, and angles of incidence α stated in ISO 4037–3 are presented in figure C6 and table D6 in appendixes C and D, respectively. The mentioned figure also shows the data used in [6] taken from [62] for $E < 10$ keV and from [63] for other photon energies. For $E < 10$ keV, the RD was typically within ±1% except for $E = 3$ keV, where the photons are, due to their low energy, already significantly affected by scattering and absorption before reaching the scoring volume; therefore, even small differences in the radiation transport parameters used by different authors, such as the cross-sections, may result in markedly different CCs. For higher energies, the RD varied within ±2.5% at $\alpha \leqslant 15°$, while for larger angles the RD varied from −5% to +10% (except for 10 keV and 75° with an RD of −12%).

A closer comparison of $h_{pK}(0.07; E, \alpha)_{slab}$ for $E \geqslant 10$ keV revealed an error in the ISO 4037-3 [6] data. The values of $h_{pK}(0.07; E, \alpha)_{slab}$ presented in [63] are denoted with an incorrect depth d and incorrect angle of radiation incidence α in ISO 4037-3. Correctly, the $h_{pK}(0.07; E, \alpha)_{slab}$ values provided in ISO 4037-3 are valid for the depth $d = 0$ mm and $\alpha = 15°$, 30°, 45°, 60°, 75°, and 82.5° according to the data given in [63], instead of $d = 0.07$ mm and $\alpha = 0°$, 15°, 30°, 45°, 60°, and 75°, respectively, as stated in ISO 4037-3, table 33 [6]. This is also the reason for the apparent outliers at $E = 10$ keV at all angles, because the depth and angle have the largest influence on the CC value at the lowest E. When the results for $h_{pK}(0.07; E, \alpha)_{slab}$ from this work and those published in [63] are compared for the correct d and α, the following RDs valid for all α are obtained: −0.4% to +0.7% for $E \geqslant 50$ keV (except for $E = 70$ keV with RD systematically around +1.6% assumed to be caused by the interpolation method) and 0.2% to 1.6% for $E < 50$ keV. These RDs are comparable to the RDs obtained for other CCs in this work. $h_{pK}(0.07; E, \alpha)_{slab}$ values were given for collision

air kerma in [63], but they are stated for the total air kerma in [6], obtained by applying g_a values from [5] to the original data, i.e. by multiplication with $(1–g_a)$.

Another set of $h_{pK}(0.07; E, \alpha)_{slab}$ values in the E range from 5 keV to 1 MeV was provided in [13], which was taken from an unpublished study [64]. Compared to the data from this work, the RD stayed within $\pm 0.5\%$ for $E \geqslant 50$ keV and for all α. For lower photon energies, the RD varied between -0.6% and $+1.9\%$ for all α. This comparison confirms that the $h_{pK}(0.07; E, \alpha)_{slab}$ values for mono-energetic photons provided in ISO 4037-3 [6] were adopted incorrectly from the original publication and should be updated.

3.3.4. $h_{pK}(3; E, \alpha)_{cyl}$

The calculated values of $h_{pK}(3; E, \alpha)_{cyl}$ from K_a to $H_p(3)$ for mono-energetic and parallel photon radiation, the cylinder phantom, and angles of incidence α stated in ISO 4037-3 are presented in figure C7 and table D7 in appendixes C and D, respectively. The mentioned figure also shows the data used in [6] taken from [8] for $E < 10$ keV and from [65] for other photon energies. A very good agreement was achieved within $\pm 1\%$ for 10 keV $< E \lesssim 2$ MeV. Slightly larger RD values were obtained for lower photon energies; however, for all such energies, the CC value was <0.06 Sv Gy^{-1}, therefore the discrepancies might be dominated by statistical uncertainties. Larger RD values up to 1.5% were observed for $E \gtrsim 2$ MeV.

According to a statement in section 2.3.2 in [65], the total air kerma was considered. This was confirmed by a comparison with results obtained by a similar group of authors in their previous publication [66], where total air kerma was used. For example, the $h_{pK}(3; E, \alpha)_{cyl}$ value for $E = 10$ MeV and $\alpha = 0°$ reported by both works differed by 0.2% only, verifying that the same approach was used. ISO 4037-3 [6] adopted the data without a correction to radiative energy losses. The cause of the discrepancy for $E \gtrsim 2$ MeV was not found, but it may be speculated that there is a possible difference between radiative energy losses in the photon cross-section table MPLIB04 [67] used in [65] and the EPRDATA library and g_a values used in the presented work.

3.3.5. $h_{pK}(10; E, \alpha)_{slab}$

The calculated values of $h_{pK}(10; E, \alpha)_{slab}$ from K_a to $H_p(10)$ for mono-energetic and parallel photon radiation, the slab phantom, and angles of incidence α stated in ISO 4037-3 are presented in figure C8 and table D8 in appendixes C and D, respectively. The mentioned figure also shows the data used in [6] taken from ICRU 57 [13] and interpolated in [16]. ICRU 57 data consist of results compiled from [63] and from unpublished work [64], which revised calculations presented in [68] originally adopted in ICRU 47 [29], all derived using collision kerma. The compilation method used in ICRU 57 is unknown. However, the RD between ICRU 57 and [63] is within $\pm 0.7\%$ for $E \geqslant 20$ keV and $\alpha \leqslant 60°$, and slightly higher otherwise. When adopted by ISO 4037-3, the CC values were corrected for radiative energy losses by applying g_a values from [5].

If ISO 4037-3 is compared to the presented work, the RD is typically within $\pm 1.5\%$ for $E > 30$ keV (or $E > 50$ keV for $\alpha = 75°$), except for a few scattered values occurring mainly for photons with $E \geqslant 3$ MeV. For low E, the RD values were much larger and reached -12%. The cause of these larger RD values is unknown but may be contributed by (a) the difference in $\frac{\mu_{en}}{\rho}$ for elements in ICRU 4-element tissue in [63] ($\frac{\mu_{en}}{\rho}$ taken from [69]) and in this work (e.g. RD of $\sim 2\%$ at $E = 10$ keV), (b) the reported statistical uncertainty of CC values up to 8% for $E \leqslant 20$ keV in [63], (c) the steep gradient of CC values for $E \lesssim 20$ keV (see figure C8) resulting in high sensitivity to radiation transport modeling and scoring of the dose quantity, (d) for $E < 10$ keV, the CC values were extrapolated as described in detail in [16] because ICRU 57 provided the CC values only for $E \geqslant 10$ keV, and (e) the CC values for $E \leqslant 12.5$ keV stated in [13] are small, and are given to one or two significant digits only, which might bias the interpolated and extrapolated CC values. As a result, the observed RD may already be relevant for dosimeter calibrations as, for example, the value presented in this study for $E = 14$ keV and $\alpha = 0°$, $h_{pK}(10; 14\text{ keV}, 0°)_{slab} = 0.183$ Sv/Gy is lower by 7.5% compared to the ISO 4037-3 one.

3.4. Summary

Source publications for mono-energetic CCs provided in ISO 4037-3 and a summary of the comparison between the presented work and that of [6] are given in table 1. Moreover, the statistical uncertainty and the uncertainty given by the selected method of calculation of the absorbed dose in this work are discussed in section 2.7.1 and in appendix B, respectively. The CC values that resulted from this work are available in electronic form [70]. A description of the files is provided in appendix A.

Table 1. Summary of ISO 4037-3:2019 [6] references for CC from air kerma to dose-equivalent quantities for mono-energetic photons and the summary of RD of CC values between this work and ISO 4037–3.

Conversion coefficient	Main reference[a]	Interpolated values[b]	Extrapolated values[b]	RD, this work[c]
$h'_K(0.07; E, \alpha)$	[13] (1998)[d]	[16] (2000)[f] [57] (2007)[f]	unclear[f]	±3% ($E \geqslant 10$ keV, $\alpha \leqslant 60°$); much larger RD for $E < 10$ keV or $\alpha > 60°$
$h'_K(3; E, \alpha)$	[54] (2017)	none	none	–1% to +0.5%
$h^*_K(10; E)$	[13] (1998)[d]	[16] (2000)	[16] (2000; $E < 10$ keV)	±3% ($E > 15$ keV); larger for $E \leqslant 15$ keV)
$h_{pK}(0.07; E)_{rod}$	[15] (1995)	[16] (2000)	[16] (2000; $E = 3$ keV)	–0.5% to +1.5%
$h_{pK}(0.07; E)_{pill}$	[15] (1995)	none	none	–0.6% to +1.1%
$h_{pK}(0.07; E, \alpha)_{slab}$	[63] (1995; $E \geqslant 10$ keV)[e] [62] (1991; $E < 10$ keV)	none	none	±1% (3 keV $< E <$ 10 keV) ±2.5% ($E \geqslant 10$ keV and $\alpha \leqslant 15°$)[e]; –5% to +10% (other E and α)[e]
$h_{pK}(3; E, \alpha)_{cyl}$	[65] (2012)	none	[8] (2012; $E < 10$ keV)	±1% (10 keV $< E \lesssim 2$ MeV); –1.5% to 0% ($E \gtrsim 2$ MeV); larger for $E \leqslant 10$ keV
$h_{pK}(10; E, \alpha)_{slab}$	[13] (1998)[d]	[16] (2000)	[16] (2000)	±1.5% ($E > 30$ keV and $\alpha \leqslant 60°$, or $E > 50$ keV and $\alpha = 75°$); up to −12% for lower E

[a] Main reference stated in [6].

[b] Reference stated in [6] for interpolated/extrapolated data of main reference.

[c] RD between this work and [6], outliers not considered; for details see plots in appendix C.

[d] ICRU 57 data were taken from various previously published literature.

[e] Incorrect data were adopted in [6] from the source publication [63].

[f] References stated in [6]. However, [57] does not include $h'_K(0.07; E, \alpha)$ for mono-energetic photons. ISO 4037-3 uses some of the interpolated values given in [16], but other interpolated values and all extrapolated values differ from those provided in [16].

3.5. Correction for the use of other photoeffect cross-sections

Some MC users may calculate K_a using a different $\frac{\mu_{en}}{\rho}$ data set for air, e.g. using PENELOPE or the renormalized XCOM libraries. To obtain the same numerical value of the appropriate dose-equivalent quantity according to equation (3) as with the $\frac{\mu_{en}}{\rho}$ data set for air and CC values used in the presented work, an energy-dependent correction needs to be applied (equation (4)), assuming that the radiative energy losses in air, $g_a(E)$, are the same:

$$K_a(E) = K_{a,Y}(E) \cdot \frac{\left(\frac{\mu_{en}(E)}{\rho}\right)_{XCOM}}{\left(\frac{\mu_{en}(E)}{\rho}\right)_{Y}}. \tag{4}$$

For PENELOPE and renormalized XCOM data sets from ICRU 90, the numerical values of the correction are provided in the supplementary file described in appendix A and visualized in figure 4. In equation (4), for a photon energy E, $K_a(E)$ is the total air kerma calculated in this paper derived with the XCOM unrenormalized $\left(\frac{\mu_{en}(E)}{\rho}\right)_{XCOM}$ data set for air, and $K_{a,Y}(E)$ is the total air kerma calculated with a different $\left(\frac{\mu_{en}(E)}{\rho}\right)_{Y}$ data set for air. It is worth noting that, what concerns K_a measurements with a primary method, the K_a value derived from free-air chamber measurements does not depend on $\frac{\mu_{en}}{\rho}$ [71], with the exception of correction factors derived with MC simulations; however, it is stated that the impact on the K_a value is not significant except for the correction for air attenuation [42]. In contrast, for air kerma cavity standards, a correction similar to equation (4) would need to be applied because $\frac{\mu_{en}}{\rho}$ occurs in the corresponding formula for K_a [72]. However, as the ratio $\left(\frac{\mu_{en}}{\rho}\right)_{air} / \left(\frac{\mu_{en}}{\rho}\right)_{graphite}$ is used, the difference introduced by the normalization screening correction partially cancels out as for both data sets, $\left(\frac{\mu_{en}}{\rho}\right)_{air}$ and $\left(\frac{\mu_{en}}{\rho}\right)_{graphite}$,

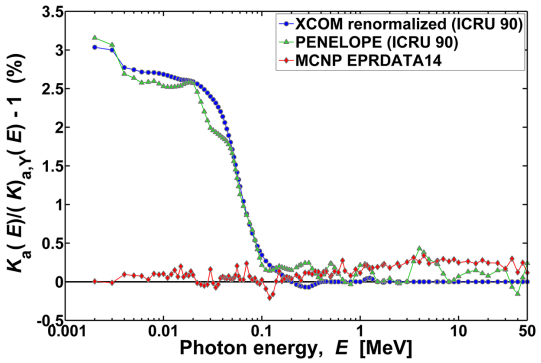

Figure 4. RD between K_a used in this paper to calculate conversion coefficient values and $K_{a,Y}$ if determined using XCOM renormalized $\frac{\mu_{en}(E)}{\rho}$ values for air from ICRU 90 (blue circles), PENELOPE $\frac{\mu_{en}(E)}{\rho}$ values for air from ICRU 90 (green triangles), and internally by MCNP with EPRDATA14 cross-section tables (red diamonds).

renormalized values are available in ICRU 90. Therefore, the RD of these ratios determined with unrenormalized and renormalized data sets does not exceed 1.1%, with the maximum RD reached at $E = 15$ keV.

4. Conclusions

New calculations of CCs from the total air kerma to all operational dosimetric quantities used for individual and area monitoring included in the ISO 4037-3:2019 standard were performed by means of MC simulations in the MCNP code for mono-energetic photons from 2 keV to 50 MeV using kerma approximation, assuming secondary CPE. As a finer energy resolution (1 keV steps up to 20 keV, 2 keV steps up to 60 keV, 5 keV steps up to 100 keV, 10 keV steps up to 200 keV, and larger steps above 200 keV) and a wider energy range (from 2 keV up to 50 MeV) was used in this work, the results allow a more accurate determination of mean CCs for radiation qualities. This is especially the case for CCs for which the tabulated values were obtained by extrapolation or interpolation from the ICRU 57 data (which only provided data from 5 keV to 1 MeV, e.g. for $h_{pK}(0.07; E, \alpha)_{slab}$, or 10 keV to 10 MeV for $h_{pK}(10; E, \alpha)_{slab}$), having higher or unspecified statistical uncertainties in the original works, or when the tabulated values are scarce, and therefore the type of interpolation significantly influences the resulting CC value. An example of the latter are extreme differences for $h'_K(0.07; E, \alpha)$ below 10 keV and for $\alpha \geqslant 75°$ as those values are zero in ICRU 57.

It was confirmed that the ISO 4037-3:2019 values of mono-energetic CCs are given for the total air kerma. The exceptions are $h'_K(0.07; E, \alpha)$, $h_{pK}(0.07; E)_{rod}$, and $h_{pK}(0.07; E)_{pill}$. However, this seems to be intended as these CCs were provided in the energy range up to 1.25 MeV only, where the radiative energy losses are assumed negligible.

The values of $h_{pK}(0.07; E, \alpha)_{slab}$ presented in ISO 4037-3:2019 were incorrectly adopted from the original publication and should be updated. In addition, some observed RDs between the presented and tabulated CCs reached values relevant for dosimeter calibrations, such as, for example, $h_{pK}(10; E, \alpha)_{slab}$ at low photon energies. Another example is the RD between the presented and the interpolated ISO 4037 $h^*_K(10; E)$ values for the main energies of photons of ^{137}Cs and ^{60}Co, which reached -2.8% ($h^*_K(10; E)$ in this work is lower).

The presented new calculations contribute to the improvement of the accuracy in radiation protection dosimetry, and the results might be considered in the upcoming update of the ISO 4037 standard. The impact of the newly calculated CCs for mono-energetic photons on the average CCs for ISO 4037-1:2019 reference radiation qualities will be detailed in a future publication.

Data availability statement

The data that support the findings of this study are openly available at the following URL/DOI: https://doi.org/10.5281/zenodo.14849038.

Acknowledgments

The project 22NRM07 GuideRadPROS received funding from the European Partnership on Metrology, co-financed from the European Union's Horizon Europe Research and Innovation Programme and by the Participating States (10.13039/100019599). Funded by the European Union. Views and opinions expressed are, however, those of the author(s) only and do not necessarily reflect those of the European Union or EURAMET. Neither the European Union nor the granting authority can be held responsible for them. This work was also partly funded by an Institutional Subsidy for Long-Term Conceptual Development of a Research Organization granted to the Czech Metrology Institute by the Ministry of Industry and Trade of the Czech Republic. The authors are grateful to George Winterbottom (PTB) for an English check of the manuscript.

The authors are very grateful to those colleagues who have contributed over decades to obtain the best possible conversion coefficients for dosimetry and radiation protection quantities and whose works have been the pillars of the present study.

Appendix A. Electronic version of conversion coefficients

CC values calculated and presented in this paper are available in electronic form. Two files are provided:

- File 1: A simple file with sheets containing tables with CC values from appendix D and the numerical values for data sets presented in figure 4 is available online [70];
- File 2: A file with comprehensive tables, where it is possible to select a quantity, phantom, depth, and angle of radiation incidence, and the CC values are shown in a table together with the tabulated CC values from [6] and their RDs. The selection of combinations of a quantity, phantom, depth, and angle of radiation incidence beyond those stated in ISO 4037-3 is possible. This file is available from the main author upon request. Additional data are presented there:
    - o CC values calculated for smaller scoring volumes are provided for quantities defined in the ICRU sphere.
    - o CC values calculated for the rotation of a phantom around the axis transversal to both the direction of radiation incidence and the phantom cylindrical axis are provided for rod, pillar, and cylinder phantoms; this axis passed through the intersection of the phantom surface and the radius opposing the direction of the radiation field.
    - o CC values calculated for smaller irradiation fields (circular field with a diameter of 10 cm and 20 cm) are provided for rod, pillar, and cylinder phantoms for $\alpha = 0°$ of the incidence of the radiation field and for the slab phantom for all α considered in [6].
    - o Numerical values for data sets presented in figure 4.

Both Excel files also contain a short description of MC simulations and visualizations of the MC models.

Appendix B. Selection of tally to calculate absorbed dose

There are several ways to calculate an estimate of the absorbed dose in MCNP radiation transport code. The selection of a suitable tally depends on the aim of the MC simulation, types of particles used and generated, particle energies, availability of cross-section data, etc [53]. To increase the calculation speed, the CCs in this work were obtained for kerma approximation in the conditions of CPE. Therefore, electrons were not transported, and only photon transport was considered. To ensure that the dose in ICRU tissue calculated with photon-only transport is reliable, different tally definitions were tested by comparison with anticipated reference values of the absorbed dose, which is derived by 'the dose tally', the *F8-tally type, when the electron transport was turned on and in the condition of CPE. Tested tallies are presented in table B 1. A simple geometry was used. A cylinder was filled with ICRU 4-element tissue. A thin, scoring volume was located inside the cylinder in a depth corresponding to 1.5 times the continuous slowing down approximation (CDSA) range for electrons with an energy equal to the energy of primary photons. The CDSA range is the average path length traveled by an electron as it slows down to rest, and its value was taken from ESTAR database [73]. Such depth was sufficient to achieve CPE.

The results obtained for energies 0.15 MeV, 0.662 MeV, 1.25 MeV, 10 MeV, 20 MeV, and 30 MeV are presented in table B2. The absolute values are not important; therefore, the results are presented as the RD to the results obtained with the *F8:P,E tally (no. 1 in table B1).

Table B1. List of tallies considered for calculation of absorbed dose in tissue.

No.	Tally	Electron transport	Tally description	Reasoning
1	*F8:P,E	On	The difference between the sum of energies entering and leaving the scoring volume. Electron transport used nearest group boundary ('Integrated Tiger Series-style') energy-indexing algorithm [53] (card DBCN 17j 1).	Expected true value. This is assumed to be the most accurate way to calculate the absorbed dose in MCNPX.
2	*F8:P,E	On	Same as no. 1; electron transport used bin-centered ('MCNP-style') energy-indexing algorithm [53]. Default for MCNPX.	To check the difference between electron transport algorithms.
3	*F8:P,E	On	Same as no. 1; calculated with MCNP 6.3 [53]. Electron transport used detailed energy- and step-specific Landau straggling sampling logic, which is default for MCNP 6.3 [53].	To check the difference between electron transport algorithms and MCNP codes.
4	F6:P	On	Photon track-length estimator of average D in a scoring volume using kerma factors from photon cross-sections.	Expected to be the same value as no. 1.
5	F6:P	Off	Same as no. 4.	Tally selected for CC calculations presented in this work.
6	F6:P	Off	Same as no. 4; calculated with MCNP 6.3 [53] with the same cross-section libraries.	To check the difference between MCNP codes.
7	+F6	Off	Total energy deposition from all particles [53].	Alternative for no. 5.
8	F4:P +FM	Off	Photon fluence converted to kerma using a tally multiplier card (fluence multiplied with the atom density, air mass in the scoring volume, the photon total cross-section, and the photon kerma factor [51]), definition: FM4 −1 m −5 −6; m = material number.	Alternative for no. 5.
9	F4:P +DE/DF	Off	Photon fluence multiplied by energy-dependent function defined as $E \cdot \left(\frac{\mu_{en}(E)}{\rho}\right)_{XCOM}$ unrenormalized (taken from [41]) to get collision kerma and hence D.	Collision kerma calculated from fluence using $\frac{\mu_{en}}{\rho}$ from [74].

The findings valid for the calculations relevant for this paper are as follows:

- *F8:P,E tally values for absorbed dose calculated with MCNPX nearest group boundary energy-indexing algorithm for electron transport agree within 0.3% with the MCNP 6.3 default Landau straggling algorithm. However, the values are higher by up to 2% compared to the MCNPX default bin-centered algorithm.
- *F8:P,E tally and F6:P tally values calculated by MCNPX 2.7.E differ by less than 0.8% if the bin-centered algorithm is used for electron transport, or exceeds that value for $E \geqslant 10$ MeV and increases up to 1.5% at $E = 30$ MeV if the nearest group boundary algorithm is used.
- F6:P tally in photon-only transport calculation results in the same value as in the coupled photon/electron transport calculation.
- F6:P tally and +F6 tally provide equivalent results.

Table B2. RD between the absorbed dose obtained with the *F8-type tally calculated by MCNPX 2.7.E and other tallies, Fx, presented as Fx/(*F8)−1, for several photon energies. Statistical uncertainty is <0.01% for F4 and F6 tallies and 0.03% for *F8 tallies, respectively.

Compared tally	RD to *F8-type tally calculated by MCNPX 2.7.E					
	150 keV	662 keV	1.25 MeV	10 MeV	20 MeV	30 MeV
*F8:P,E (no. 2 in table B 1)	0.04%	−0.36%	−0.90%	−1.30%	−1.82%	−1.70%
*F8:P,E (MCNP 6.3, no. 3 in table B 1)	0.01%	0.26%	0.34%	−0.05%	0.09%	0.02%
F6:P (with electron transport)	0.05%	−0.17%	−0.49%	−0.89%	−1.09%	−1.50%
F6:P	0.05%	−0.16%	−0.49%	−0.82%	−1.05%	−1.53%
F6:P (MCNP 6.3)	0.05%	−0.17%	−0.49%	−0.82%	−1.03%	−1.49%
+F6	0.05%	−0.16%	−0.49%	−0.82%	−1.05%	−1.53%
F4:P + FM	0.05%	−0.14%	−0.45%	−0.12%	0.98%	2.22%
F4:P + DE/DF	0.15%	−0.55%	−0.70%	−3.35%	−5.97%	N/A[a]

[a] $\frac{\mu_{en}(E)}{\rho}$ not available for $E = 30$ MeV in XCOM database [74].

- F6:P tallies calculated with MCNPX 2.7.E and MCNP 6.3 codes using the same cross-section tables provide equivalent result.
- F4:P + DE/DF tally agrees with F6:P tally at lower energies but is lower for higher photon energies; the explanation is that this tally is defined in such a way that it is lacking radiative energy losses and counts collision energy losses only.
- F4:P+FM tally provides higher results than F6:P; the difference is even larger with respect to F4:P+DE/DF. However, this difference closely corresponds to $(1 - g_a)$ values.

Therefore, for the calculations relevant for this paper, it is concluded that:

- It is not the aim of this paper to evaluate differences in electron energy loss methods available in MCNP codes. It was decided that the dose calculation tallies in this Appendix would be compared to the 'expected true value' of the absorbed dose obtained with the more recent electron transport algorithm available in the MCNPX code, which uses the nearest group boundary method for the calculation of electron energy losses.
- F6:P tally in photon-only transport calculation is a good estimate of the absorbed dose in tissue: the systematic uncertainty given by the difference between the absorbed dose obtained with the *F8-type tally and the kerma approximation of absorbed dose obtained with the F6:P-type tally is 0.05% at 150 keV, 0.2% at 662 keV, 0.5% at 1.25 MeV, 0.8% at 10 MeV, 1.1% at 20 MeV, and 1.5% at 30 MeV under CPE.
- F4:P +FM is the total kerma.

As a result, the F6:P tally in photon-only transport calculations was used to derive the absorbed dose value in the phantoms and the F4:P tally with the FM multiplier (FMx −1 m −5 −6, x = tally number, m = material number) was used to check the analytical determination of the total air kerma obtained using equation (1).

Appendix C. Plots of conversion coefficients

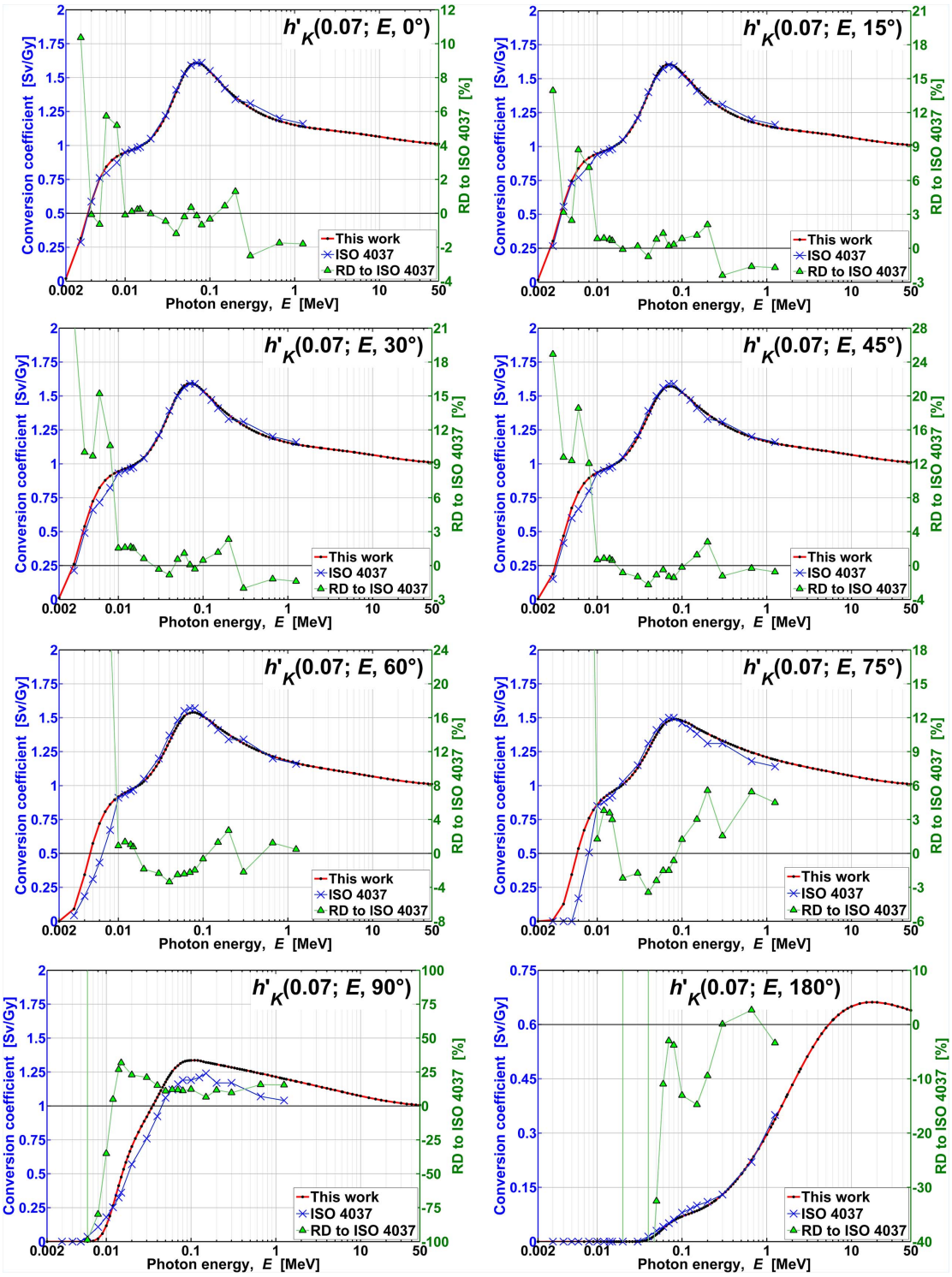

Figure C1. Values for $h'_K(0.07; E, \alpha)$ for various angles of radiation incidence, α, calculated in this study, h_{MC} (red line), published in ISO 4037–3:2019, h_{ISO} (blue crosses), and their relative difference, RD = h_{MC}/h_{ISO}-1, at energies where values of both data sets were available (triangles, right axis).

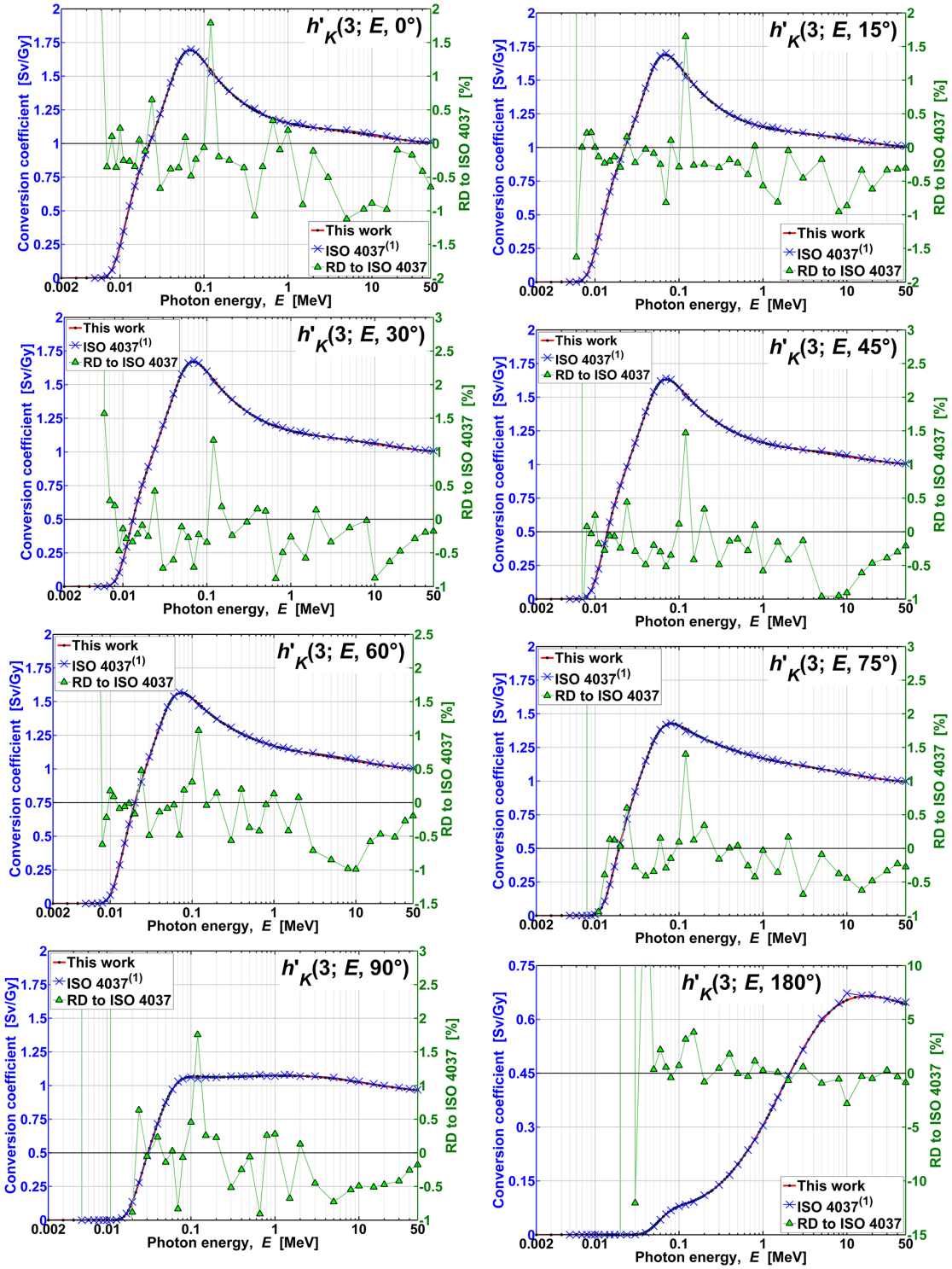

Figure C2. Values for $h'_K(3; E, \alpha)$ for various angles of radiation incidence, α, calculated in this study, h_{MC} (red line), published in ISO 4037–3:2019, h_{ISO} (blue crosses), and their relative difference, RD $= h_{MC}/h_{ISO}$-1, at energies where values of both data sets were available (triangles, right axis). (1) Blue cross values for $E > 10$ MeV were taken from [54], table A2, and corrected for $(1 - g_a)$ values [50] used in the presented paper.

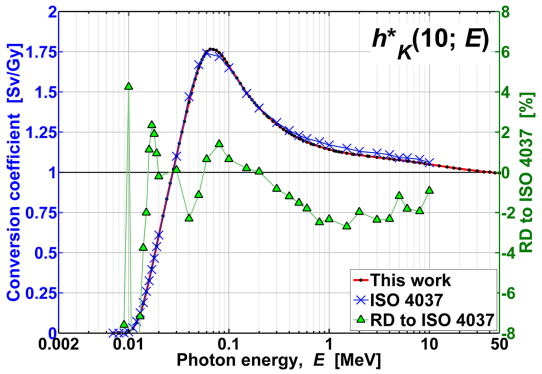

Figure C3. Values for $h^*_K(10; E)$ calculated in this study, h_{MC} (red line), published in ISO 4037–3:2019, h_{ISO} (blue crosses), and their relative difference, RD = $h_{MC}/h_{ISO}-1$, at energies where values of both data sets were available (triangles, right axis).

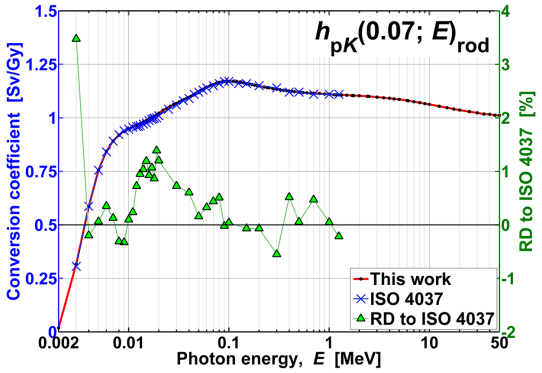

Figure C4. Values for $h_{pK}(0.07; E)_{rod}$ for the rod phantom calculated in this study, h_{MC} (red line), published in ISO 4037–3:2019, h_{ISO} (blue crosses), and their relative difference, RD = $h_{MC}/h_{ISO}-1$, at energies where values of both data sets were available (triangles, right axis).

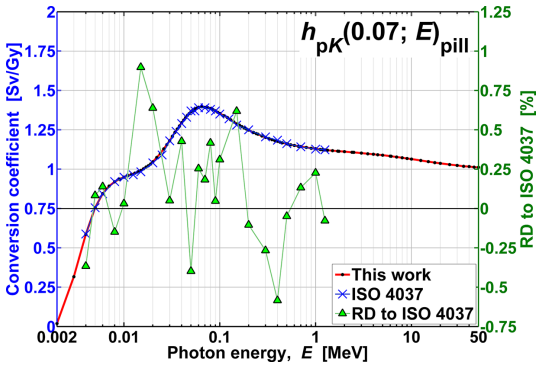

Figure C5. Values for $h_{pK}(0.07; E)_{pill}$ for the pillar phantom calculated in this study, h_{MC} (red line), published in ISO 4037–3:2019, h_{ISO} (blue crosses), and their relative difference, RD = $h_{MC}/h_{ISO}-1$, at energies where values of both data sets were available (triangles, right axis).

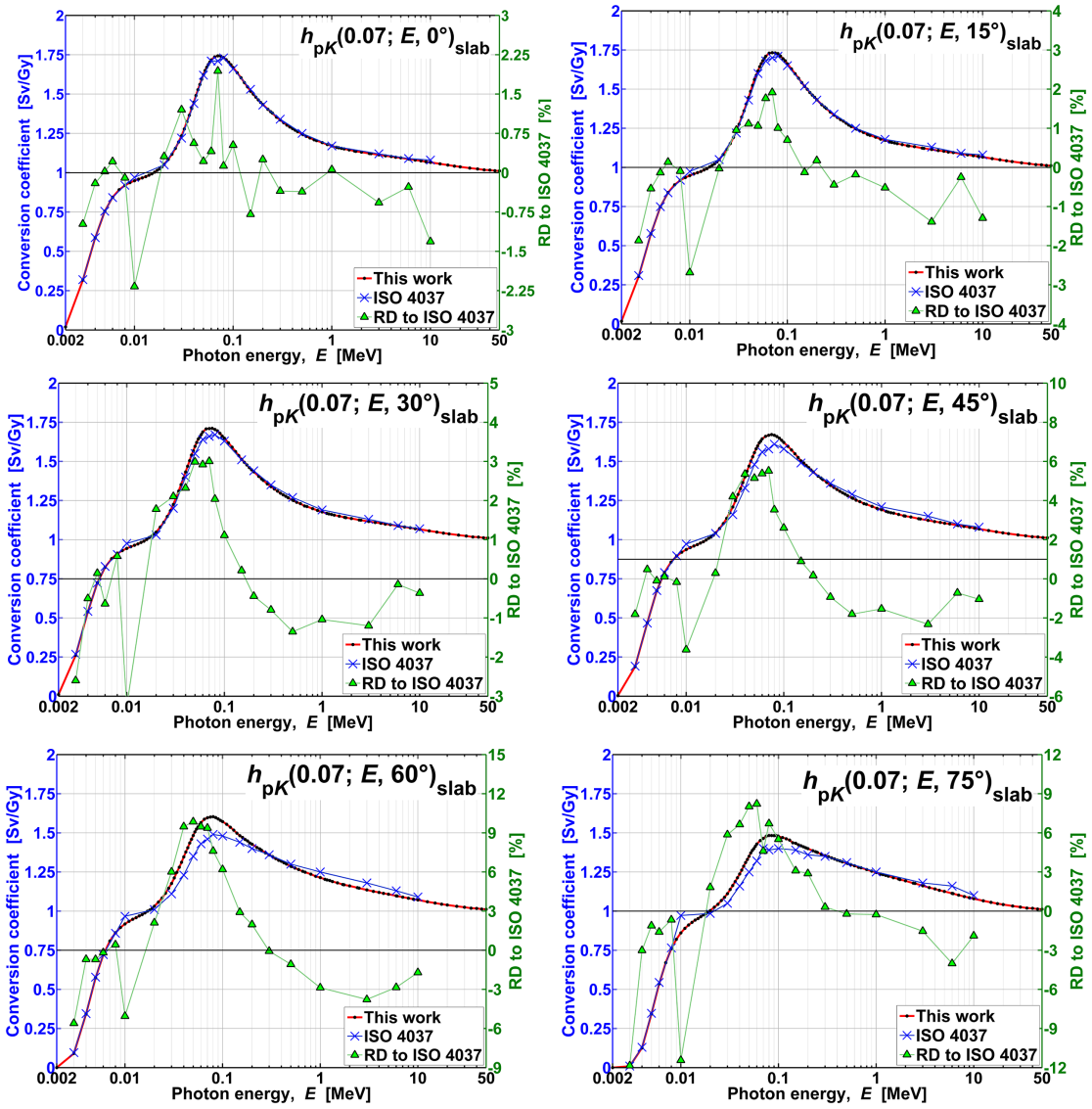

Figure C6. Values for $h_{pK}(0.07; E, \alpha)_{slab}$ for the slab phantom for various angles of radiation incidence, α, calculated in this study, h_{MC} (red line), published in ISO 4037–3:2019, h_{ISO} (blue crosses), and their relative difference, RD = $h_{MC}/h_{ISO} - 1$, at energies where values of both data sets were available (triangles, right axis).

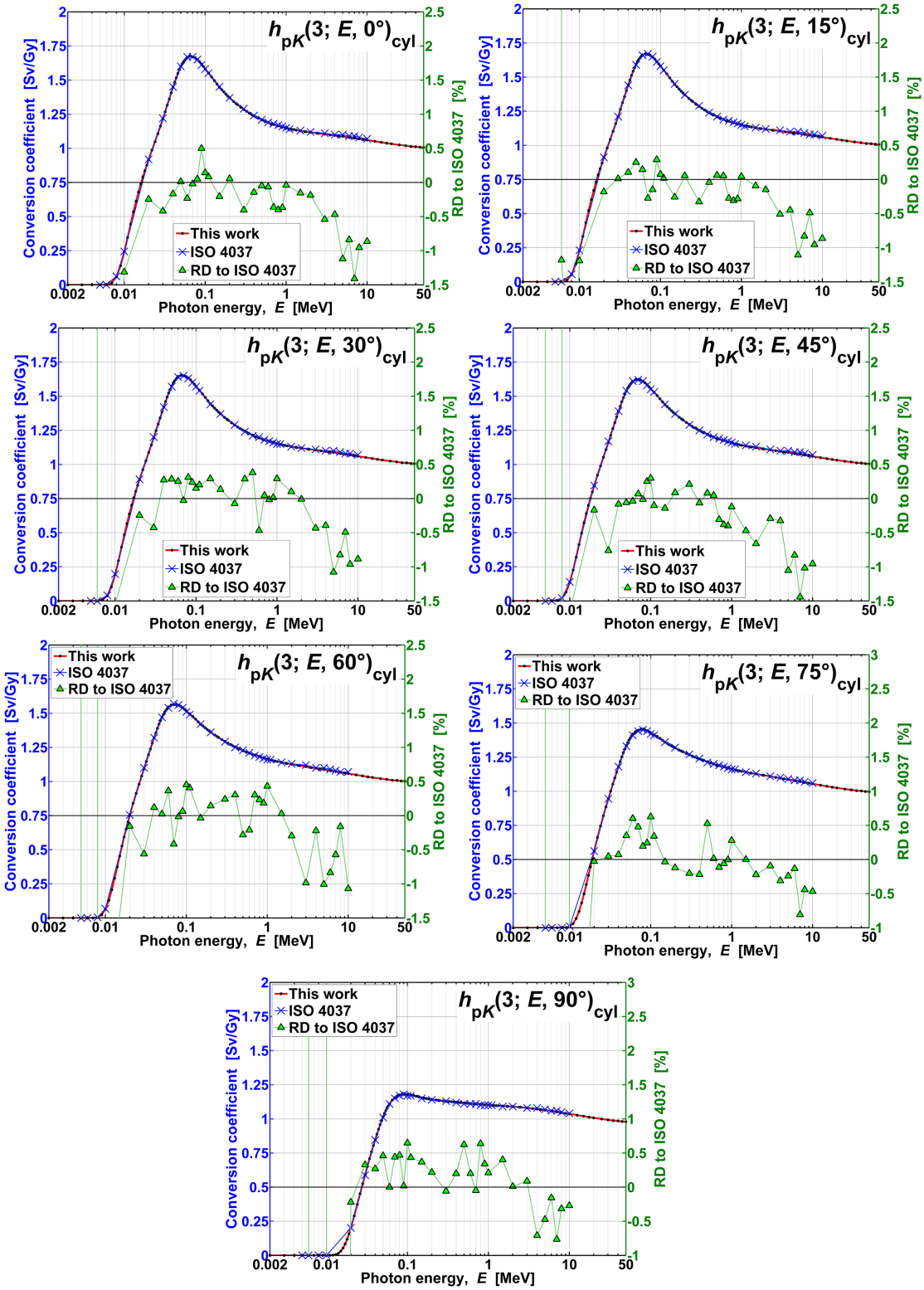

Figure C7. Values for $h_{pK}(3; E, \alpha)_{cyl}$ for the cylinder phantom for various angles of radiation incidence, α, calculated in this study, h_{MC} (red line), published in ISO 4037–3:2019, h_{ISO} (blue crosses), and their relative difference, RD = $h_{MC}/h_{ISO} - 1$, at energies where values of both data sets were available (triangles, right axis).

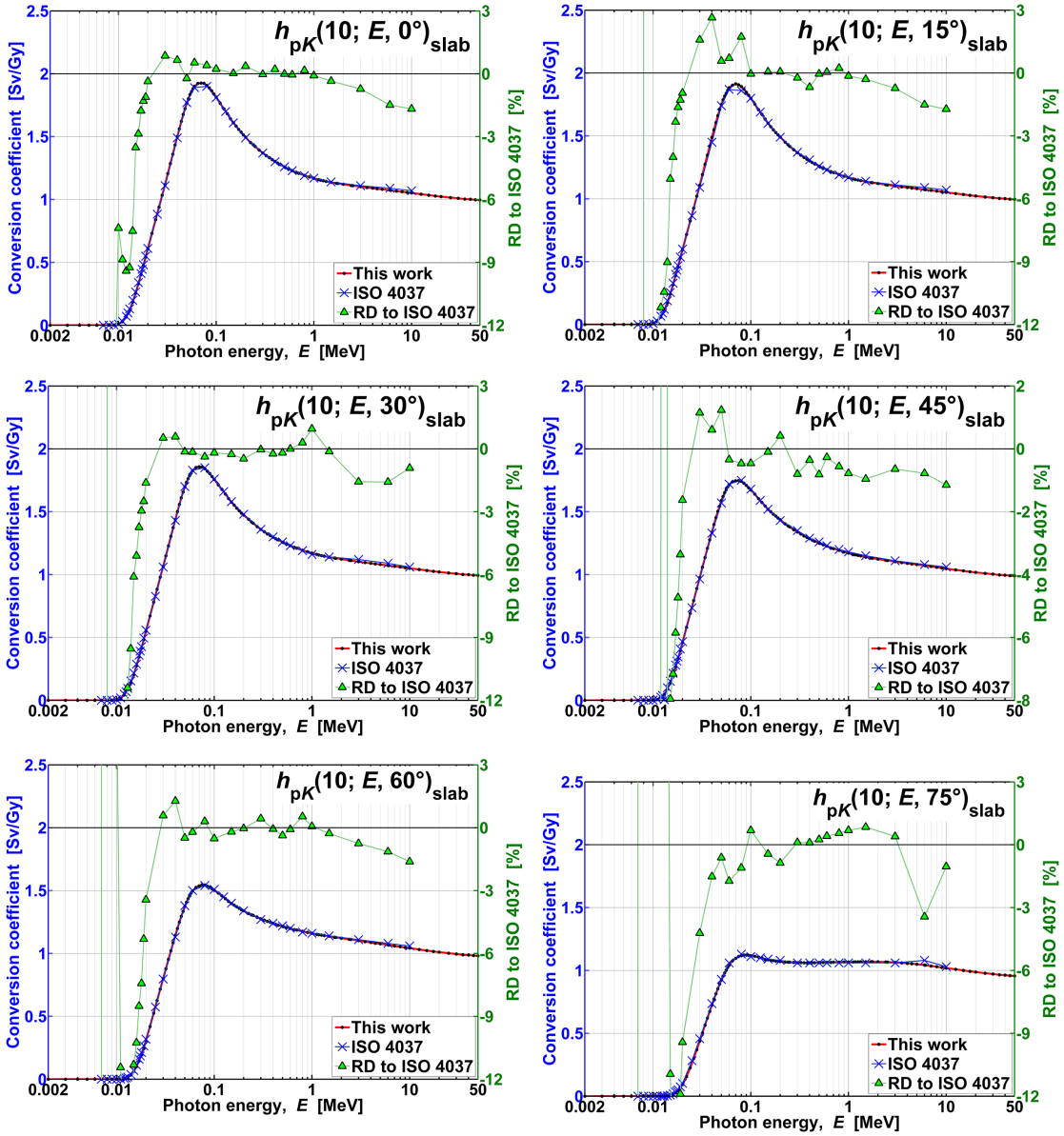

Figure C8. Values for $h_{pK}(10; E, \alpha)_{slab}$ for the slab phantom for various angles of radiation incidence, α, calculated in this study, h_{MC} (red line), published in ISO 4037–3:2019, h_{ISO} (blue crosses), and their relative difference, RD = $h_{MC}/h_{ISO} - 1$, at energies where values of both data sets were available (triangles, right axis).

Appendix D. Tables of conversion coefficients

The tables are provided in the supplementary Excel file [70] only, because they are very large.

Table D1: conversion coefficients $h'_K(0.07; E, \alpha)$ from total air kerma, K_a, to the directional dose-equivalent $H'(0.07)$ for mono-energetic and parallel photon radiation (expanded and aligned field) as calculated in this study: see sheet 'Table D1_H'(0.07)' in supplementary Excel file [70].

Table D2: conversion coefficients $h'_K(3; E, \alpha)$ from total air kerma, K_a, to the directional dose-equivalent $H'(3)$ for mono-energetic and parallel photon radiation (expanded and aligned field) as calculated in this study: see sheet 'Table D2_H'(3)' in supplementary Excel file [70].

Table D3: conversion coefficients $h^*_K(10; E)$ from total air kerma, K_a, to the ambient dose-equivalent $H^*(10)$ for mono-energetic and parallel photon radiation (expanded and aligned field) as calculated in this study: see sheet 'Table D3_Hamb(10)' in supplementary Excel file [70].

Table D4: conversion coefficients $h_{pK}(0.07; E)_{rod}$ from total air kerma, K_a, to the dose-equivalent $H_p(0.07)$ for mono-energetic and parallel photon radiation (expanded and aligned field) and the rod phantom at angle of radiation incidence of 0° as calculated in this study: see sheet 'Table D4_H_p(0.07)rod' in supplementary Excel file [70].

Table D5: conversion coefficients $h_{pK}(0.07; E)_{pill}$ from total air kerma, K_a, to the dose-equivalent $H_p(0.07)$ for mono-energetic and parallel photon radiation (expanded and aligned field) and the pillar phantom at angle of radiation incidence of 0° as calculated in this study: see sheet 'Table D5_H_p(0.07)pill' in supplementary Excel file [70].

Table D6: conversion coefficients $h_{pK}(0.07; E, \alpha)_{slab}$ from total air kerma, K_a, to the dose-equivalent $H_p(0.07)$ for mono-energetic and parallel photon radiation (expanded and aligned field) and the ICRU slab phantom as calculated in this study: see sheet 'Table D6_H_p(0.07)slab' in supplementary Excel file [70].

Table D7: conversion coefficients $h_{pK}(3; E, \alpha)_{cyl}$ from total air kerma, K_a, to the dose-equivalent $H_p(3)$ for mono-energetic and parallel photon radiation (expanded and aligned field) and cylinder phantom consisting of ICRU tissue as calculated in this study: see sheet 'Table D7_H_p(3)cyl' in supplementary Excel file [70].

Table D8: conversion coefficients $h_{pK}(10; E, \alpha)_{slab}$ from total air kerma, K_a, to the dose-equivalent $H_p(10)$ for mono-energetic and parallel photon radiation (expanded and aligned field) and the ICRU slab phantom as calculated in this study: see sheet 'Table D8_H_p(10)slab' in supplementary Excel file [70].

ORCID iDs

Jaroslav Šolc https://orcid.org/0000-0002-1629-5697
Paz Avilés Lucas https://orcid.org/0009-0002-1577-7122
Luka Bakrač https://orcid.org/0000-0001-6756-6672
Rolf Behrens https://orcid.org/0000-0002-4905-7791
Alessia Ciccotelli https://orcid.org/0000-0002-7643-1195
N Cornejo Díaz https://orcid.org/0000-0001-6757-4998
Steffen Ketelhut https://orcid.org/0000-0003-2099-3452
Nikola Kržanović https://orcid.org/0000-0002-9210-5840
Massimo Pinto https://orcid.org/0000-0002-8122-7084
Teemu Siiskonen https://orcid.org/0000-0002-4471-6938
Vladimír Sochor https://orcid.org/0009-0000-4181-560X
Jiří Tesař https://orcid.org/0000-0002-5691-4050
Joonas Tikkanen https://orcid.org/0000-0002-4005-4885
Dušan B Topalović https://orcid.org/0000-0001-5976-963X
Olivier Van Hoey https://orcid.org/0000-0002-6649-2138
Hayo Zutz https://orcid.org/0000-0002-0907-6509
Miloš Živanović https://orcid.org/0000-0003-2965-1897

References

[1] ICRP 103, International Commission on Radiological Protection (ICRP) 2007 The 2007 Recommendations of the International Commission on Radiological Protection. ICRP publication 103 *Ann. ICRP* **37** 2–4
[2] ICRU 39, International Commission on Radiation Units and Measurements (ICRU) 2007 Determination of dose equivalents resulting from external radiation sources *ICRU Report* vol 39 (Bethesda)
[3] ICRU 51, International Commission on Radiation Units and Measurements (ICRU) 1993 Quantities and units in radiation protection dosimetry *ICRU Report 51* (Bethesda)
[4] ISO 4037-1:2019 2019 *X and Gamma Reference Radiation for Calibrating Dosemeters and Doserate Meters and for Determining their Response as a Function of Photon Energy. Part 1: Radiation Characteristics and Production Method ISO 4037-1, Geneva* (International Organization for Standardization (ISO))

[5] ISO 4037-2:2019 2019 *X and Gamma Reference Radiation for Calibrating Dosemeters and Doserate Meters and for Determining their Response as a Function of Photon Energy. Part 2: Dosimetry for Radiation Protection Over the Energy Ranges 8 KeV to 1.3 MeV and 4 MeV to 9 MeV ISO 4037-2, Geneva* (International Organization for Standardization (ISO))
[6] ISO 4037-3:2019 2019 *X and Gamma Reference Radiation for Calibrating Dosemeters and Goserate Meters and for Determining their Response as a Function of Photon Energy. Part 3: Calibration of Area and Personal Dosemeters and the Measurement of their Response as a Function of Energy and Angle of Incidence ISO 4037-3, Geneva* (International Organization for Standardization (ISO))
[7] ISO 4037-4:2019 2019 *X and Gamma Reference Radiation for Calibrating Dosemeters and Doserate Meters and for Determining their Response as a Function of Photon Energy. Part 4: Calibration of Area and Personal Dosemeters in Low Energy x Reference Radiation Fields ISO 4037-4, Geneva* (International Organization for Standardization (ISO))
[8] Behrens R 2012 Air kerma to $H_p(3)$ conversion coefficients for a new cylinder phantom for photon reference radiation qualities *Radiat. Prot. Dosim.* **151** 450–5
[9] ISO 4037-3:1999 1999 *X and Gamma Reference Radiation for Calibrating Dosemeters and Dose Rate Meters and for Determining Their Response as a Function of Photon Energy. Part 3: Calibration of Area and Personal Dosemeters and the Measurement of their Response as a Function of Energy and Angle of Incidence ISO 4037-3, Geneva* (International Organization for Standardization (ISO))
[10] Ankerhold U, Berens R and Ambrosi P 1999 X-ray spectrometry of low energy photons for determining conversion coefficients from air kerma, ka, to personal dose equivalent, $H_p(10)$, for radiation qualities of the ISO narrow spectrum series *Radiat. Prot. Dosim.* **81** 247–58
[11] Hakanen A, Kosunen A, Poyry P and Tapiovaara M 2007 Determination of conversion factors from air kerma to operational dose equivalent quantities for low-energy x-ray spectra *Radiat. Prot. Dosim.* **125** 198–204
[12] Kharrati H and Zarrad B 2004 Computation of conversion coefficients relating air Kerma to $H_p(0.07,alpha)$, $H_p(10,alpha)$, and $H^*(10)$ for x-ray narrow spectrum from 40 to 140 kV *Med. Phys.* **31** 277–84
[13] ICRU 57, International Commission on Radiation Units and Measurements (ICRU) 1998 Conversion coefficients for use in radiological protection against external radiation *ICRU Report 57* (Bethesda)
[14] Wagner S R, Grosswendt B, Selbach H-J, Siebert B R L, Harvey J R and Mill A J 1985 Unified conversion functions for the new ICRU operational radiation protection quantities *Radiat. Prot. Dosim.* **12** 231–5
[15] Grosswendt B 1995 Angular-dependence factors and air kerma to dose equivalent conversion coefficients for cylindrical phantoms irradiated by plane-parallel extended monoenergetic photon beams *Radiat. Prot. Dosim.* **59** 165
[16] Ankerhold U 2000 Catalogue of x-ray spectra and their characteristic data: ISO and DIN radiation qualities, therapy and diagnostic radiation qualities, unfiltered x-ray spectra (Physikalisch-Technische Bundesanstalt (PTB)) (https://doi.org/10.7795/110.20190315B)
[17] ICRP 116, International Commission on Radiological Protection (ICRP) 2010 Conversion coefficients for radiological protection quantities for external radiation exposures. ICRP publication 116 *Ann. ICRP* **40** 1–257
[18] Behrens R 2011 Air kerma to dose equivalent conversion coefficients not included in ISO 4037-3 *Radiat. Prot. Dosim.* **147** 373–9
[19] Behrens R and Otto T 2022 Conversion coefficients from total air kerma to the newly proposed ICRU/ICRP operational quantities for radiation protection for photon reference radiation qualities *J. Radiol. Prot.* **42** 011519
[20] ICRP 110, International Commission on Radiological Protection (ICRP) 2009 Adult reference computational phantoms, ICRP publication 110 *Ann. ICRP* **38** 1
[21] ICRU 95, International Commission on Radiation Units and Measurements (ICRU) 2020 Operational quantities for external radiation exposure, ICRU report 95 *J. ICRU* **20**
[22] Bossin L, Carbonez P, Christensen J B, Furlan M, Fürholz F, Mayer S, Pitzschke A and Yukihara E G 2024 Implications of the ICRU 95 quantities for various personal dosimetry techniques *Radiat. Meas.* **176** 107207
[23] Hoedlmoser H, Bandalo V and Figel M 2020 BeOSL dosemeters and new ICRU operational quantities: response of existing dosemeters and modification options *Radiat. Meas.* **139** 106482
[24] Figel M 2024 ICRU95 and the future individual monitoring, Workshop "Fit for purpose: a German contribution to the new ICRP recommendations Munich, Germany
[25] Gilvin P *et al* 2022 Evaluation of the impact of the new ICRU operational quantities and recommendations for their practical application *EURADOS Report 2022–02* (https://doi.org/10.12768/yxy4-5q82)
[26] 22NRM07 GuideRadPROS project website (available at: https://projects.ciemat.es/web/guideradpros-euramet) (Accessed 9 January 2025)
[27] ICRU 85, International Commission on Radiation Units and Measurements (ICRU) 2011 Fundamental quantities and units for ionizing radiation (revised) *ICRU Report 85a* (International Commission on Radiation Units and Measurements)
[28] Alberts W, Ambrosi P, Böhm J, Dietze G, Hohlfeld K and Will W 1995 New dose quantities in radiation protection *PTB-Bericht Dos-23e* (Physikalisch-Technische Bundesanstalt (PTB)) (https://doi.org/10.7795/110.20200417EN)
[29] ICRU 47, International Commission on Radiation Units and Measurements (ICRU) 1992 Measurement of dose equivalents from external photon and electron radiations *ICRU Report 47*
[30] Bordy J M, Gualdrini G, Daures J and Mariotti F 2011 Principles for the design and calibration of radiation protection dosemeters for operational and protection quantities for eye lens dosimetry *Radiat. Prot. Dosim.* **144** 257–61
[31] Alberts W G *et al* 1994 Thompson international standardization of reference radiation and calibration procedures for radiation protection instruments *Proc. 26th Annual Meeting of the 'Fachverband fur Strahlenschutz e. V.'* (German-Swiss Radiation Protection Association)
[32] ICRP Publication 103 2020 Protection quantities and ICRU report 39/51 operational quantities *J. ICRU* **20** 20–23
[33] Endo A 2016 Operational quantities and new approach by ICRU *Ann. ICRP.* **45** 178–87
[34] ISO 29661:2012/Amd.1:2015, International Organization for Standardization (ISO) 2015 Reference radiation fields for radiation protection—definitions and fundamental concepts ISO 29661, 2012, Geneva and Amendment 1: ISO 29661 Amd.1
[35] Behrens R, Kowatari M and Hupe O 2009 Secondary charged particle equilibrium in ^{137}Cs and ^{60}Co reference radiation fields *Radiat. Prot. Dosim.* **136** 168–75
[36] Büermann L, Gargioni E and Kramer H-M 2001 Mixed high energy photon and electron radiation fields for calibrating radiation protection dosemeters *Radiat. Prot. Dosim.* **96** 213–7
[37] Hubbell J H and Seltzer S M 2004 Tables of x-ray mass attenuation coefficients and mass energy-absorption coefficients (version 1.4) (National Institute of Standards and Technology) (available at: http://physics.nist.gov/xaamdi) (Accessed 8 January 2025)
[38] Cullen D E 2023 EPICS2023: August 2023 status report *IAEA-NDS-0242*
[39] Sabbatucci L and Salvat F 2016 Theory and calculation of the atomic photoeffect *Radiat. Phys. Chem.* **121** 122–40

[40] Salvat F 2015 PENELOPE-2014: a code system for Monte Carlo simulation of electron and photon transport *OECD/NEA Data Bank, NEA/NSC/DOC(2015)3*
[41] ICRU 90, International Commission on Radiation Units and Measurements (ICRU) 2016 Key data for ionizing-radiation dosimetry: measurement standards and applications *ICRU Report No.* 90 (Oxford University Press)
[42] McEwen M, Burns D, Darienzo M, de Pooter J, Pinto M and Rapp B 2017 Report to CCRI(I) on the recommendations of *ICRU Report* 90, CCRI(I)/17-07
[43] Cullen D E 2018 A survey of photon cross section data for use in EPICS2017 *Report IAEA-NDS-225, rev.1*
[44] Cullen D 2024 Private Communication (Lawrence Livermore National Laboratory)
[45] Seltzer S 2024 Private Communication (National Institute of Standards and Technology)
[46] Behrens R 2017 Compilation of conversion coefficients for the dose to the lens of the eye *Radiat. Prot. Dosim.* **174** 348
[47] Pelowitz D B *et al* 2011 MCNPX 2.7.E extensions *LA-UR-11-01502* (Los Alamos National Laboratory)
[48] Werner Ch J *et al* 2018 MCNP version 6.2 release notes *LA-UR-18-20808* (Los Alamos National Laboratory)
[49] Cullen D E *et al* 1997 EPDL97: the evaluated photon data library, '97 version *UCRL-50400* (Lawrence Livermore National Laboratory) vol 6
[50] Seltzer S and Behrens R 2024 Private communications
[51] X-5 Monte Carlo Team 2003 MCNP—A general Monte Carlo N-particle transport code, version 5, volume I: overview and Theory *LA-UR-03-1987* (Los Alamos National Laboratory)
[52] Adams K J 2000 Electron upgrade for MCNP4B *Report* X-5-RN(U)-00-14 (Los Alamos National Laboratory)
[53] Kulesza J A *et al* 2022 MCNP® code version 6.3.0 theory & user manual *Report* LA-UR-22-30006, Rev. 1 (Los Alamos National Laboratory)
[54] Behrens R 2017 Conversion coefficients for $H'(3;\Omega)$ for photons *J. Radiol. Prot.* **37** 354
[55] Kawrakow I, Mainegra-Hing E, Rogers D W O, Tessier F and Walters B R B 2011 The EGSnrc code system: Monte Carlo simulation of electron and photon transport *NRCC Report* PIRS-701 (National Research Council of Canada (NRC))
[56] Dimbylow P J, Francis T M and Bartlett D T 1989 Calibration of photon personal dosimeters in terms of the ICRU operational quantities: calculations of phantom backscatter and depth-dose distributions *Report No. NRPB-R230* (National Radiological Protection Board)
[57] Ankerhold U 2007 X reference radiation qualities produced with tube voltages above 300 kV for the calibration and testing of dosemeters *Radiat. Prot. Dosim.* **123** 137–42
[58] Grosswendt B and Hohlfeld K 1982 Angular dependence of specified depth dose equivalent quantities in the ICRU sphere for photon radiation *Radiat. Prot. Dosim.* **3** 169–74
[59] Seltzer S M 1993 Calculation of photon mass energy-transfer and mass energy-absorption coefficients *Radiat. Res.* **136** 147–70
[60] Grosswendt B, Hohlfeld K, Kramer H and Selbach H-J 1988 Conversion factors for ICRU dose equivalent quantities for the calibration of radiation protection dosimeters *PTB-Dos-11 (e)* (Physikalisch-Technische Bundesanstalt (PTB))
[61] Dimbylow P J and Francis T M 1984 The calculation of dose equivalent quantities in the ICRU sphere for photon energies from 0.01 to 10 MeV *Radiat. Prot. Dosim.* **9** 49–53
[62] Grosswendt B 1991 The angular dependence and irradiation geometry factor for the dose equivalent for photons in slab phantoms of tissue-equivalent material and PMMA *Radiat. Prot. Dosim.* **35** 221–35
[63] Till E, Zankl M and Drexler G 1995 Angular dependence of depth doses in a tissue slab irradiated with monoenergetic photons *GSF-Report* 27/95
[64] Grosswendt B, Buermann L, Kramer H M, Till E and Zankl M Reference coefficients $H_p(0.07,\alpha)$ and $H_p(10,\alpha)$ from air kerma to the dose equivalent quantities in the ICRU slab (unpublished)
[65] Vanhavere F *et al* 2012 ORAMED: optimization of radiation protection of medical staff *EURADOS Report* 2012-02
[66] Daures J *et al* 2009 Conversion coefficients from air kerma to personal dose equivalent Hp(3) for eye-lens dosimetry CEA-R-6235 (CEA)
[67] White M C 2003 Photoatomic data library MCPLIB04: a new photoatomic library based on data from ENDF/B-VI release 8 *Report* LA-UR-03-1019 (Los Alamos National Lab)
[68] Grosswendt B 1990 Conversion coefficients for calibrating individual photon dosemeters in terms of dose equivalents defined in an ICRU tissue cube and PMMA slabs *Radiat. Prot. Dosim.* **32** 219–31
[69] Hubbell J H 1982 Photon mass attenuation and energy-absorption coefficients *Int. J. Appl. Radiat. Isot.* **33** 1269–90
[70] Electronic version of CC values presented in this work. Proposal for new values of ISO 4037 mono-energetic photon conversion coefficients *Zenodo online repository* (https://doi.org/10.5281/zenodo.14849038)
[71] Burns D T and Büermann L 2009 Free-air ionization chambers *Metrologia* **46** S9
[72] Büermann L and Burns D T 2009 Air-kerma cavity standards *Metrologia* **46** S24
[73] Berger M J, Coursey J S, Zucker M A and Chang J 2017 Stopping-power & range tables for electrons, protons, and helium ions *NIST Standard Reference Database 124* (NISTIR 4999) (https://doi.org/10.18434/T4NC7P)
[74] Hubbell J H and Seltzer S M2004Tables of x-ray mass attenuation coefficients and mass energy-absorption coefficients from 1 keV to 20 MeV for elements Z = 1–92 and 48 additional substances of dosimetric interest *NIST Standard Reference Database* vol 126 (NISTIR 5632)